This is to certify that the
thesis entitled

STUDY OF A NOVEL R718 TURBOCOMPRESSION CYCLE

presented by

Amir Ahmadzadeh Kharazi

has been accepted towards fulfillment
of the requirements for the

Ph.D. degree in Mechanical Engineering

N. Li

Major Professor's Signature

08/25/06

Date

MSU is an Affirmative Action/Equal Opportunity Institution

STUDY OF A NOVEL R718 TURBOCOMPRESSION CYCLE

By

Amir Ahmadzadeh Kharazi

A DISSERTATION

Submitted to
Michigan State University
in partial fulfillment of the requirements
for the degree of

DOCTOR OF PHILOSOPHY

Department of Mechanical Engineering

2006

ABSTRACT

STUDY OF A NOVEL R718 TURBOCOMPRESSION CYCLE USING A 3-PORT CONDENSING WAVE ROTOR

by

Amir A. Kharazi

Water is a natural refrigerant, which is absolutely harmless to man and nature. It is easily available and incurs no problems with its disposal after use. Even though water is one of the oldest refrigerants, state of the art technology is required to use water as a refrigerant in compression refrigeration plants with turbocompressors.

To compare water (R718) to other refrigerants, a code is developed in which all refrigerants can be compared in a single *p-h*, *T-s*, or *p-T* diagram. Using the code, the COP isolines of water (R718) and any refrigerant can be generated in a graph to determine which refrigerant has a better COP for a certain evaporation temperature and temperature lift. In regard to using water (R718) as a refrigerant, some specific features complicate its application in refrigeration plants with turbocompressors. Because the cycle works under coarse vacuum, the volumetric cooling capacity of water vapor is very low. Hence, huge volume flows have to be compressed with relatively high pressure ratios. Therefore, the use of water (R718) as a refrigerant compared to classical refrigerants, such as R134a or R12, requires approximately 200 times the volume flow, and about twice the pressure ratio for the same applications.

To enhance the turbocompression and improve the efficiency of R718 cycles, the novel concept of 3-port condensing wave rotors integrated in R718 compression refrigeration cycles is investigated. The condensing wave rotor employs pressurized water to pressurize, desuperheat, and condense the refrigerant vapor, all in one dynamic process. The underlying phenomena of flash evaporation, shock wave compression, desuperheating, and condensation inside the wave rotor channels are described in a wave and phase-change diagram as part of internal flow analysis. A characteristic equation is developed for the determination of the pressure required for the high pressure inlet port when the low pressure port and the outlet are known. For the external analysis, the thermodynamic process is described in detail. Based on the described thermodynamic model, a computer program is generated to evaluate the performance of the R718 baseline and wave-rotor-enhanced cycles. The effect of some key parameters on the performance enhancement is demonstrated as an aid for optimization. A performance map summarizes the findings and shows optimum wave rotor pressure ratio and maximum relative performance improvement of R718 cycles by using the 3-port condensing wave rotor.

Experimental investigation of the flow inside a small size wave rotor is described in the last chapter. This experimental analysis is reported as a proof of concept for wave energy exchange in smaller sizes, which ultimately lead to micro wave rotors. Moreover, the Schlieren method is used for shock wave visualization. Based on the skills developed, Shlieren technique is recommended for flow visualization in channels of a condensing wave rotor.

TO MY WIFE

ACKNOWLEDGMENTS

I am taking this opportunity to thank all those who have assisted me in one way or the other with my Ph.D. thesis.

I would like to thank professor Norbert Mueller for giving me the opportunity to work with the Turbomachinary group at the Michigan State University. The friendly and supportive atmosphere inherent to the whole Turbomachinary labratory contributed essentially to the final outcome of my studies. In this context, I would like to thank particularly for my Ph.D. committee professors Jaberi, Engeda, and MacCluer. Also, I would like to thank Pejman Akbari for his guidence during early stages of my Ph.D., with whom I published several publications.

For their hospitality, I would like to thank the wave rotor group at the University of Tokyo, where the experimental study of this thesis was conducted. I am particularly grateful to professor Charles Petty, who was so kind as to give me opportunities in the Center for Multiphase Transport Phenoma. Without his support the completion of this dissertation would not have been possible.

Expressing gratitude to persons who played a role during a Ph.D. thesis can be an unending task for even minor or seemingly unrelated contributions may affect or influence it substantially. Therefore, I would like to thank my parents, whose contribution was not related directly to the work itself but without knowing of their moral support and assurance, their found conviction in principle question of life and their strong belief, this work would not have been possible. I truly owe

everything to them, my gratitude and acknowledging their choices and decisions, which build the basis for a unique family.

Finally, I owe special thanks to my wife Mahnaz for her patience, love, and encouragement during these years of my studies.

This work received financial support from the National Science Foundation, MSU Graduate Office, and MSU Engineering Department.

TABLE OF CONTENT

LIST OF TABLES

LIST OF FIGURES

CHAPTER 1: INTRODUCTION

1.1. REFRIGERATION

Refrigeration and Air conditioning encompasses every sphere of human life. It not only provides comfortable and healthy living environments, but has also come to be regarded as necessities for surviving severe weather and preserving food. Unfortunately, accelerated technical development and economic growth in much of the world during the last century have produced severe environmental problems so that in the mid nineteen-eighties the world recognized that CFC refrigerants, once considered safe for people as well as the planet, were in fact severely damaging the Earth's ecology. Refrigerants suddenly went from being rarely discussed to a hot topic of research. Aside from cost reduction, being environmentally safe is being the biggest driving forces for technical innovation and using natural refrigerants for refrigeration.

Refrigeration is defined as "the transfer of heat from a lower temperature region to a higher temperature one" [1]. Refrigeration devices that produce refrigeration operate using the vapor-compression cycle. Heat pumps, refrigerators, automotive air-conditioners, and residential or commercial air-conditioners are examples of refrigeration devices. All of these devices have one thing in common, to reduce the temperature of an enclosed environment.

The purpose of the refrigerator is to remove heat from the cold region while requiring as little external work as possible. A measure of the efficiency of the device is therefore coefficient of performance (COP) which is equal to the rate of heat removal from the cold region to the rate work is done:

$$COP = \frac{\dot{q}}{\dot{w}} \quad (1)$$

The most common refrigeration cycle in use today is the vapor refrigeration cycle. As shown in Figure 1, the vapor compression cycle uses energy input to drive a compressor that increases the pressure of the refrigerant which is in the vapor state. The refrigerant is then exposed to the hot region in a device called a condenser. As a result, heat is transferred from the refrigerant to the hot region causing it to condense. The refrigerant then passes through the expansion valve across which its pressure and temperature drop considerably. The refrigerant temperature is now below that which exists in the cold or refrigerated region in the device called an evaporator. As a result, heat is transferred from the refrigerated region to the refrigerant causing it to pass from the liquid state to the vapor state again. The refrigerant then again passes to the compressor in which its pressure is increased and the whole cycle is repeated.

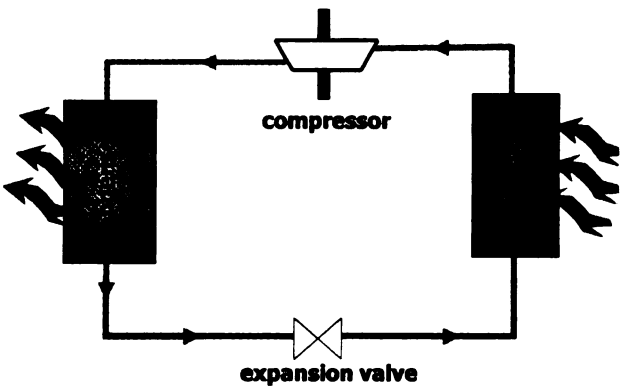

Figure 1: Basic compression refrigeration cycle

1.2. NATURAL REFRIGERANTS

In 1974, scientists published a laboratory study on ozone layer depletion by chlorofluorocarbon (CFC) refrigerants, solvents, aerosol product propellants and foam blowing agents [2]. Further studies estimated that the ozone layer would be depleted by CFCs by about 7% within 60 years. Based on such studies the US has banned CFCs in aerosol sprays since 1978. By the mid-1980s, the overall concern about CFCs was raised again when scientists discovered that CFCs were also efficient greenhouse gases. In 1984-1985, Japanese and British scientists discovered that the ozone layer above the Antarctic was dangerously depleted. Therefore, urgent action was needed to prevent increasing skin cancer, cataracts, suppression of the human immune system, and destruction of crops and natural ecosystems [3]. United Nations Environment Program (UNEP) coordinated the unprecedented response, involving scientists, engineers, industry, environmental pressure groups and the public, as well as international agencies, governments and diplomats. In 1985, the first general ozone agreement, known as the Vienna Convention for the Protection of the Ozone Layer, was a pledge to protect the ozone layer [4]. The specific commitments came in 1987 through the Montreal Protocol signed by fifty seven industrial nations. The 1987 Montreal Protocol has been progressively strengthened several times for the rapid phase-out of the production and consumption of ozone depleting substances [5].

Since the Montreal Protocol, there has been a tremendous effort among the refrigeration and air-conditioning industry to find the best substitute for CFCs now

under phase out [6,7]. The search for new and environmentally benign refrigerants has renewed interest in natural refrigerant technologies. Although natural refrigerants were used extensively in the early years of refrigeration technology, a number of technical and safety challenges caused them to be readily abandoned when CFCs became available. These challenges still exist today for air, ammonia, hydrocarbons, carbon dioxide, and water.

Air (R729) is used extensively as a refrigerant in air-conditioning in aircrafts and train compartments (Figure 2). The use of air as a refrigerant is based on the principle that when a gas expands isentropically from a given temperature, its final temperature at the new pressure is much lower. The resulting cold gas, in this case air, can then be used as a refrigerant [8]. Air-cycle systems are compact and lightweight. However, the efficiency of such systems is quite poor and is mainly limited by the efficiencies of compression and expansion devices, as well as those of the heat exchangers employed. The air refrigeration cycles appear to use more energy than comparable vapor compression cycles [9].

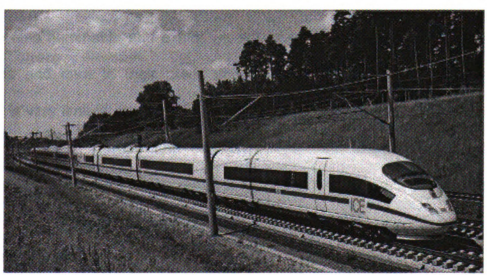

Figure 2: The German Deutche Bahn ICE-1 train, air conditioned with compressed air as refrigerant

Ammonia (R717) has been the most widely used natural refrigerant. After more than a century using ammonia as a refrigerant, a tremendous amount of practical experience exists with this refrigerant. There is no doubt about its superior thermodynamic and transfer properties compare to other available refrigerants. However, because of its high toxicity and flammability, thorough care should be paid in handling and such systems require more preventive maintenance [10]. For instance, the US Occupational Health and Safety Administration (OSHA) considers ammonia as a hazardous material, and imposes certain regulations on its use, storage, handling and occupational exposure [11]. As a result, the applications of ammonia are mostly limited to large warehouses where it can be strictly managed such as at a plant.

Hydrocarbons (HC) are appropriate refrigerants in many ways including energy efficiency, critical point, solubility, transport, and heat transfer properties [12]. For refrigeration applications, a number of hydrocarbons such as propane (R-290), n-butane (R-600) and isobutene (R600a) are suitable to use. However, they are also flammable and explosive, which causes the need for changes in standards and care in their production. The use of hydrocarbons in North America is very limited; because of restrict laws for flammability risks. However, some countries in Europe and elsewhere have less-stringent liability laws. Nevertheless, the danger of fire remains an overriding concern. To address this challenge with safety features, the cost of a system would have to be increased by about one-third [13].

Carbon Dioxide (R744) has very low toxicity and operates at very high pressures which sound promising for systems that must be small and light-weight, such as automotive or portable air conditioners. Carbon Dioxide systems are "transcritical" meaning the compressed gas out of compressor must be cooled against a heat sink temperature that is usually above the critical temperature [14]. Because of the nature of the transcritical cycle, the efficiency of Carbon Dioxide is quite poor (low specific cooling capacity) requiring more energy for compression [15].

Water is a natural and clean refrigerant with no Ozone Depletion Potential (ODP=0), no contribution to the global warming (GWP=0), and without any safety risk. It is chemically stable, nontoxic, nonflammable, commonly available, and easily disposable after use. In R718 systems, water serves as both refrigerant and heat transfer fluid. Therefore, direct heat exchangers can be used for evaporator and condenser increasing the energy-saving potential. Moreover, water can function as a working fluid for refrigeration and heat pump cycles in the range of evaporation temperature of 0 °C to very high temperatures (e.g. 150 °C). Even though water is one of the oldest refrigerants, state of the art technology is required to use water as a refrigerant in absorption chillers or in compression chillers with steam injection compressors. These techniques are energy efficient as long as there is waste heat or steam available. Much higher energy efficiency can be achieved using compression refrigeration plants with turbocompressors.

Water has been used as a refrigerant for air-conditioning and for the production of ice, using steam ejectors, large centrifugal compressors, and large

high-speed axial compressors. The future of water as a refrigerant for vapor compression refrigeration depends either on the innovative designs of the cycle or development of high-speed axial compressors to operate at the very low pressures required for R718 refrigerating.

The key component of a R718 turbochiller is the compressor, since water as a refrigerant has some specific features that complicate its application in refrigeration plants with turbocompressors. Since the cycle works under coarse vacuum, the volumetric cooling capacity of water vapor is very low. Hence, huge volume flows have to be compressed with relative high pressure ratios. Therefore, the use of water (R718) as a refrigerant ,compared to classical refrigerants, such as R134a or R12, requires approximately 200 times the volume flow, and about twice the pressure ratio for the same applications. Because of the thermodynamic properties of water vapor, this high pressure ratio requires approximately a two to four times higher compressor tip speed, depending on the impeller design; while the speed of sound is approximately 2.5 times higher. Reynolds numbers are about 300 times lower and the specific work transmission per unit of mass has to be around 15 times higher.

This states challenges for the compressor design. Today they are successfully solved in commercial industrial plants mainly installed in Europe using unique high-performance mixed-flow turbocompressors with or without stationary guide vanes. Other concepts are under investigation, like mixed flow compressors with inducer or pre-runner or axial multistage compressors, promising a higher pressure ratio or a more compact design. High pressure ratios

are obtained by the combination of high rpm and large diameter, where the diameter is primarily limited by the available space and manufacturing facility. Working under vacuum the forces exerted by the gas on blades are very small. So the blades must primarily withstand centrifugal forces resulting from their inherent mass allowing for more economic lightweight constructions with extremely thin, mostly straight blades, made of special materials like titanium or composites. These impellers are very much different from usual high-performance impellers. They cannot be milled. They are built of several parts, indicating a challenge for manufacturing and balancing of the high-speed system. Advantageous is the use of variable speed direct-drive motors, working under vacuum and water vapor atmosphere, requiring special bearing, cooling and electrical isolation. Such motors are not readily available and need to be developed for each new power level. Furthermore R718 turbochillers have a lower noise emission and require no special safety installation concerning drainage and ventilation. R718 turbochillers represent a cutting edge technology, which is challenging and rewarding. They allow a move towards greener technology with a huge potential for application and manufacturing even outside of Europe [16]. If R718 cycles are successfully developed, one can imagine that many toxic and polluted sources, such as urban waste water, could be a valuable source of energy for refrigeration or heat pumps.

1.3. WATER AS A REFRIGERANT

There has been a tremendous effort by the refrigeration and air-conditioning industry to find the best substitute for chlorofluorocarbon (CFC) refrigerants [6,

7]. The search for new and environmentally benign refrigerants has renewed interest in technologies that use natural refrigerants, such as water (R718). Considering all pros and cons of natural refrigerants already described in previous studies [17, 18], water can be considered as an attractive refrigerant because of its following advantages:

- It has no global warming potential (GWP=0).
- It has no ozone depletion potential (ODP=0).
- It is nontoxic, nonflammable, easy to handle, and inert to the environment (minimizes safety precautions).
- It has no risk of future restrictions due to refrigerant environmental impact.
- It creates no disposal problem after use.
- It works with very low pressure differences, reducing safety precautions.
- It has high theoretical coefficient of performance (COP), competitive with CFCs depending on the evaporation temperature [19, 20].
- The system working with water as a refrigerant can use direct heat exchangers for evaporation and condensation. Therefore, R718 systems can obtain very high COP [21].
- Tap water, treated waste water, or coarsely filtered river water can be used directly as make-up water (warehousing bulky refrigeration canisters is not required).
- Chiller systems, coupled with a closed cooling-tower loop, allow for diminished water treatment.

- Turbochillers using water as a refrigerant have shown to be inherently much less noisy than conventional compression chiller systems.

Despite the above attractive features, there are a few challenges of using water as a refrigerant compared to traditional refrigerants. At the triple point, the vapor pressure of water is only 611 Pa, which $<1\%$ of the atmospheric pressure. The low operating pressures of water-vapor refrigeration systems combined with the steep vapor pressure curve of water requires compression systems that can handle large-volume flows while still delivering high-pressure ratios [22-25]. This states challenges for the compressor design. Although single-stage turbocompressors commonly deliver large-volume flows with mostly insufficient pressure ratios, positive displacement compressors can obtain high-pressure ratios but only for relative small-volume flows. A technical compromise has been the use of multistage turbocompressors with intercooler [26]. The drawback of multistage compressors with intercoolers is being spacious.

For the reasons described, R718 hardly competes with other commonly used refrigerants in small household size refrigeration or air-conditioning applications. Any affordable cycle modification or newly invented device which could simultaneously handle large volume flows while still achieving high pressure ratios will give R718 an edge over other commonly used refrigerants.

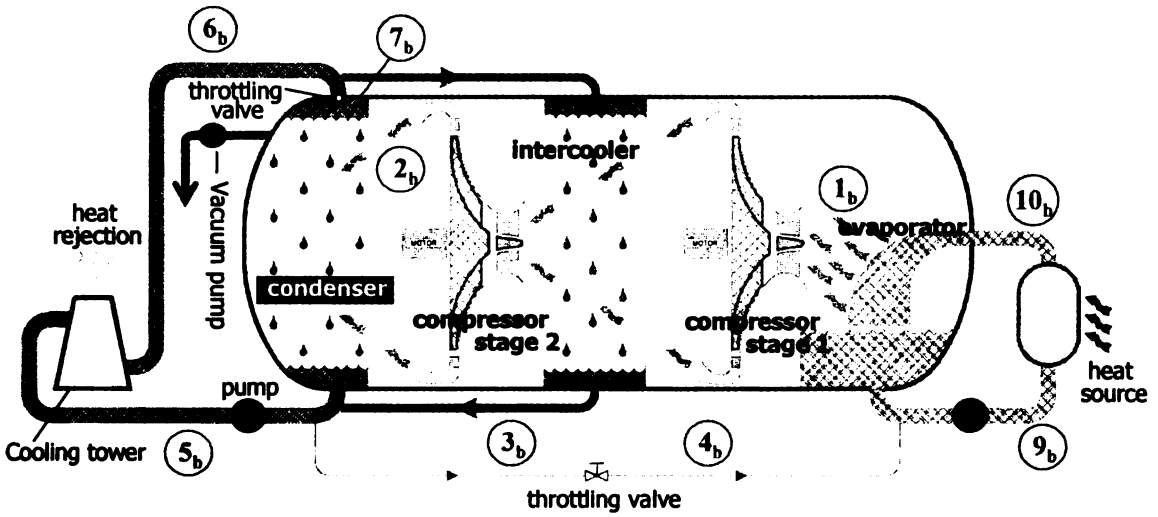

Figure 3: Schematic of a R718 chiller unit with direct condensation and evaporation

Figure 3 pictures the schematic of a two-stage R718 turbochiller with direct condensation and evaporation, two high-performance centrifugal compressors, and an intercooler. Figure 4 is a schematic thermodynamic model for the actual system.

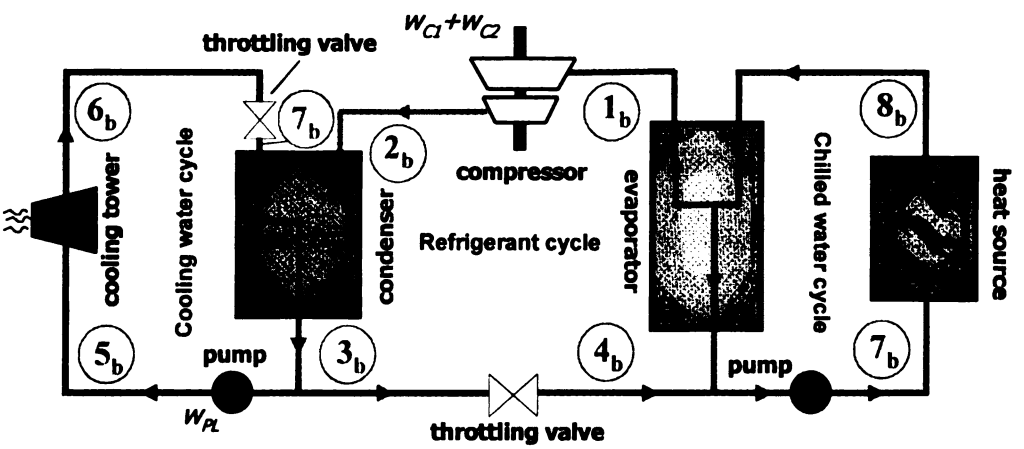

Figure 4: Schematic of thermodynamic model of a R718 chiller unit with a two-stage compressor and a direct condenser

R718 units can be comprised of three directly interlinked cycles: (i) a cooling water cycle that condenses the superheated vapor from the compressor and releases the thermal energy to the ambient through a heat exchanger device, mostly a cooling-tower; (ii) a chilled water cycle that absorbs thermal energy from the heat source and transfers it to the refrigerant by phase change; (iii) a refrigerant cycle or the core cycle that consists of four components: compressor, expansion device, condenser, and evaporator. Cooling-towers can be direct (open-circuit) or indirect (closed-circuit) heat rejection equipment. In the direct type, cooling water is exposed directly to the atmosphere. The warm cooling water is sprayed over a fill that increases the contact area, and air is blown through the fill. The majority of heat removed from the cooling water is because of partial evaporation of the cooling water requiring a permanent replenishment. The remaining cooled water drops into a collection basin and is recirculated to the chiller. Using such an open circuit, a pump is required before the cooling-tower to pump the water out of condenser at subambient pressure to somewhat above ambient pressure. In this case, considerable throttling occurs after the cooling-tower when the water enters the condenser under vacuum, which is shown by a throttling valve in Figure 3. The use of direct heat exchangers may result in contamination of the refrigerant with noncondensable gases, solids, or entrained liquids [24]; therefore, using indirect heat exchangers may reduce the cost associated with degasifiers and cleaning. There are two options for realization, which can be used alternatively or combined. First, an indirect cooling-tower can be employed in which water circulates through tubes (coils)

located in the tower without coming in contact with the outside air and pressure. The cooling-tower heat transfer still may be enhanced as needed by wetting the outside of the coils utilizing evaporative cooling. If an indirect cooling-tower (closed circuit) is used, the pump needs only to overcome the pressure loss in the cooling circuit and throttling losses at the entrance to the evaporator can be minimized. In such a case the pump can be placed before or after the cooling-tower, depending on where pump cavitation is prevented best considering the competing effects of temperature drop and pressure loss across the cooling-tower. Second, the cooling-tower can be separated from the chiller unit using effective plate heat exchangers. These typically introduce only 1 K additional temperature difference that adds to the ~1 K temperature difference in the internal direct heat exchanger (condenser). This is still superior to an internal indirect condensing heat exchanger, which may typically introduce a temperature difference of ~5 K.

Disadvantages of the current state-of-the-art R718 units (Figure 3) are mainly their size and cost. The size is because of the use of two centrifugal compressors with comparably large diameters and voluminous (same diameter) internal direct heat exchangers. The cost is mainly generated by the two relative expensive compressors with independent variable speed drives. An additional challenge has been obtaining high peak compressor pressure ratios for high temperature-lifts. One reason has been the limited compressor efficiency that results from the special wheel construction and the limited pressure recovery of the steady-state diffuser which decelerates the high-speed vapor flow out of the high-performance

wheel. Low Reynolds numbers of water vapor under vacuum (300 times lower than if R134a or R12 are used) [25] are an additional challenge for achieving a high efficiency.

Although water as a refrigerant has been known for a long time, related research and commercial use has been exploited only recently, using mechanical vapor compression mechanism [28]. Compressors [29], considered for water vapor compression technology, are usually axial compressors [30], centrifugal compressors, cycloid compressors

[31], roots and liquid ring compressors [32], and jet ejectors [33,34]. As an example for the use of axial compressors the HydroFrio™, chiller has been introduced by INTEGRAL [35]. HydroFrio™ was projected to consist of a flash evaporator, direct contact condenser, and an axial compressor, which is used as water chiller, ice water chiller, binary ice generator (VacuumICE©), heat pump, and cascades. IDE (IDE Technologies Ltd.) of Israel has been the leader in commercial centrifugal water vapor compression technology. IDE often uses two stage compressors to reach the required temperature lift and pressure ratio [36]. With financial support from the Danish Energy Agency (DEA), the Sabroe Refrigeration Company and DTI have used the IDE centrifugal compressors to build a refrigeration plant, using solely water as refrigerant in the compression process [37]. INTEGRAL has also used IDE centrifugal compressors for research and installations [35]. The IDE centrifugal compressors have been developed into two products called ECOVIM and ECO-CHILLER. The ECO-VIM (Vacuum Ice Machine) is used to condense the water vapor to ice [38]. The ECO-CHILLER

removes heat from the water by direct flashing to producing chilling [39]. Figure 5 shows examples of chillers with 100-300 ton capacity commercialized in Europe.

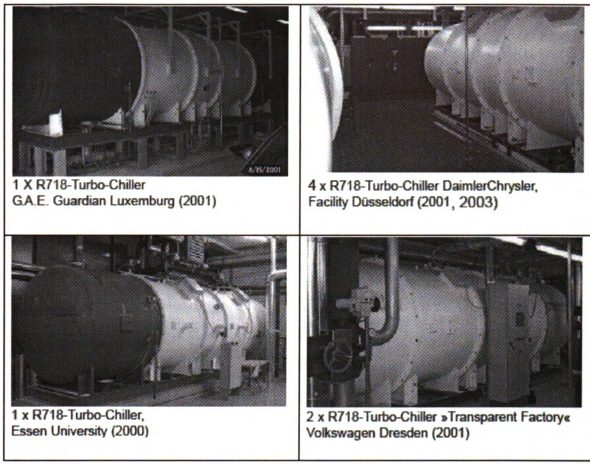

Figure 5: 100-300 ton chillers commercialized in Europe

Following an intensive multi-year developing effort, Institut für Luft- und Kältetechnik (ILK) Dresden, over the last years has successfully commercialized its modern chillers with now multiple units operating in Europe such as those at the Volkswagen and DaimlerChrysler factories in Germany and GAE Gardian Luxemburg. To the best knowledge of the author, all commercial turbocompression systems using water as a refrigerant built so far have been in large scale and a need for smaller units, in an economical and efficient solution,

exists. The presented work is part of the ongoing research to improve the compressors and heat exchangers and to reduce the size and cost of the whole unit.

CHAPTER 2: COMPARATIVE INVESTIGATION OF WATER AS A REFRIGERANT

2.1. COMPARISON IN A TEMPERATURE PRESSURE DIAGRAM

Figure 6 compares water to other common refrigerants in the pressure-temperature diagram. Water has a very high critical point compare to other refrigerants, which makes it a competitive refrigerant in heat pump applications. One restriction when using water as a refrigerant is that it is restricted to applications in which the cooling requirements are above its freezing point (0°C), if no antifreeze additives are added.

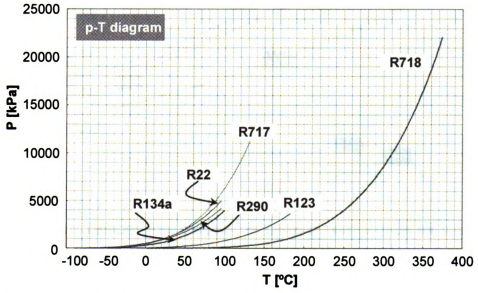

Figure 6: Pressure-Temperature diagram for common refrigerants

Figure 7 is again the Pressure-Temperature diagram zoomed in common refrigeration operating range. As shown in this graph, water works in sub-ambient pressure and its p-T curves lies under all other investigated refrigerants.

Although water works with very low pressure differences, its low pressure operating point cause higher pressure ratios in the compressor. A rule of thumb for refrigerants is that as lower the evaporator pressure, as higher the pressure ratio of the compressor.

Table 1 shows the required compressor pressure ratios for several refrigerants in a simple compression refrigeration cycle. R718 requires 2 to 3 times higher compressor pressure ratio when is used in a typical compression refrigeration cycle.

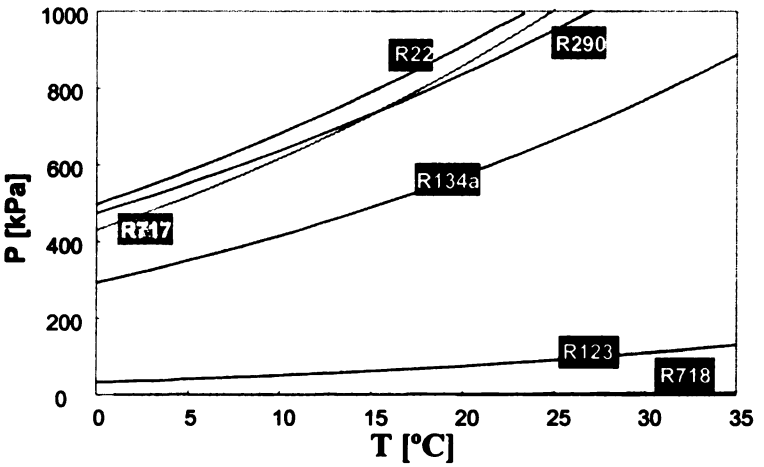

Figure 7: Pressure-Temperature diagram for common refrigerants for a common refrigeration operating range

Refrigerant	R22	R290	R717	R134	R123	R718
Compression Ratio (T_e = 5°C, T_c = 35°C)	2.3	2.2	2.6	2.5	3.19	6.45

Table 1: Required compressor pressure ratio for several refrigerants

2.2. COMPARISON IN A TEMPERATURE ENTROPY DIAGRAM

Figure 8 is the comparison between investigated refrigerants in a temperature-entropy diagram. As shown in the picture, water (R718) has a wide dome compare to the other refrigerants. Therefore, when used in a refrigeration cycle during evaporation and condensation, entropy change is significant. This means, for example in the evaporator, water molecules need a large amount of energy to enter the gaseous phase. This fact does not necessarily mean a higher COP for water because; a higher pressure ratio is needed in the compressor. On the other hand, higher energy gain during evaporation means in each cycle of refrigerant water, a significant amount of energy can be removed from the refrigeration compartment compared to the other refrigerants with the same mass flow rate. Therefore, for a fixed refrigeration capacity, water works with a lower mass flow rate compare to other common refrigerants.

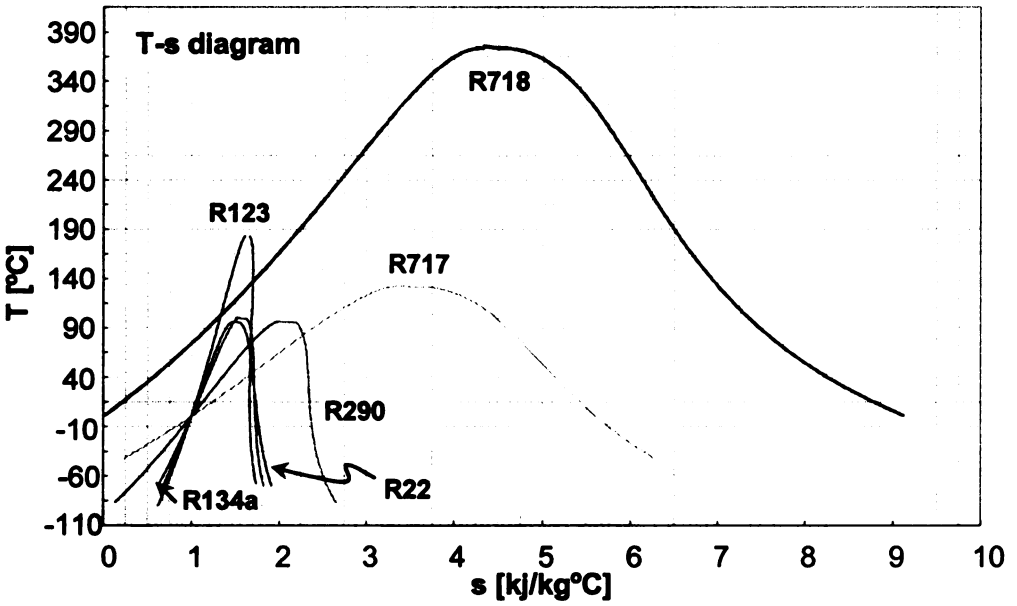

Figure 8: Temperature-Entropy diagram for common refrigerants

In refrigeration cycles, Carnot standard cycle is considered an "ideal" cycle. If a Carnot cycle is considered operating between evaporation and condensation

temperature, any deviation from ideality is considered irreversibility of the cycle. With this assumption, the irreversibility of a simple refrigeration cycle comes from two internal sources: desuperheating and throttling.

Figure 9 shows the irreversibility associated with desuperheating and throttling for a typical refrigeration cycle. Based on this graph, the entropy production during desuperheating process is

$$s_{prod.} = \frac{h_b - h_c}{T_{cond.}} - (s_b - s_c) \tag{2}$$

, and the entropy production during throttling is

$$s_{prod.} = s_f - s_d \tag{3}$$

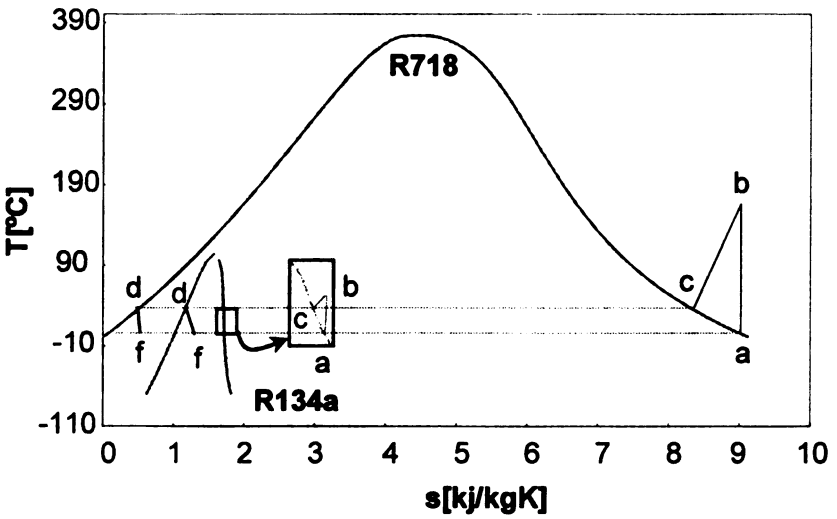

Figure 9: Entropy production during desuperheating and throttling for R718 and R134a

2.2.1 DESUPERHEATING AND THROTTLING IRREVERSIBILITY FACTORS

To compare irreversibility of different refrigerants, two factors are to be introduced: desuperheating factor and throttling factor.

For desuperheating, two parameters contribute to irreversibility of a refrigeration cycle. One is the inclination of constant pressure lines in a T-s diagram and the other one is the entropy change during desuperheating. The following is the derivation of constant pressure lines inclination in superheated region for any refrigerant.

The differential form of the second law of thermodynamics is

$$ds = \frac{dq}{T} \tag{4}$$

which indicates that the change in entropy is equal to the inverse of the temperature integrated over the heat transferred.

Using the first law of thermodynamics $de = dq - dw$, the definition of work for a gas $dw = pdV$, and the enthalpy definition $h = e + pV$, the differential change in heat transferred can be written as

$$dg = dh - Vdp \tag{5}$$

which shows an alternative way of presenting the first law of thermodynamics.

Equation of state for an ideal gas is

$$T = \frac{pV}{R} \tag{6}$$

For a constant pressure process based on equation 5, $dq = dh$. Also, the heat transferred for a gas is defined as heat capacity of the gas times the change in temperature.

$$dq = CdT \tag{7}$$

Therefore,

$$dh = C_p dT \tag{8}$$

,where C_p is the heat capacity in constant pressure. Substituting 8 in 5, and its result and 6 in 4, the following relation is obtained

$$ds = C_p \frac{dT}{T} - R\frac{dp}{p} \tag{9}$$

Equation 9 can then be integration from state "2" to state "3" to give

$$\Delta s = (C_p)_{ave} \ln\frac{T_2}{T_3} - R\ln\frac{p_2}{p_3} \tag{10}$$

For an isobaric process, equation 10 simplifies to

$$\Delta s = (C_p)_{ave} \ln\frac{T_2}{T_3} \tag{11}$$

Figure 10 shows a zoomed region around saturation vapor line for a refrigerant. During an isobaric process from T_2 to T_3, the slope of constant pressure line is

$$\tan\alpha = \frac{T_2 - T_3}{\Delta s} \tag{12}$$

Substituting equitation 11 to equitation 12, the following equitation is obtained

$$\tan\alpha = \frac{T_2 - T_3}{\dfrac{\ln T_2 - \ln T_3}{(C_p)_{ave}}} \tag{13}$$

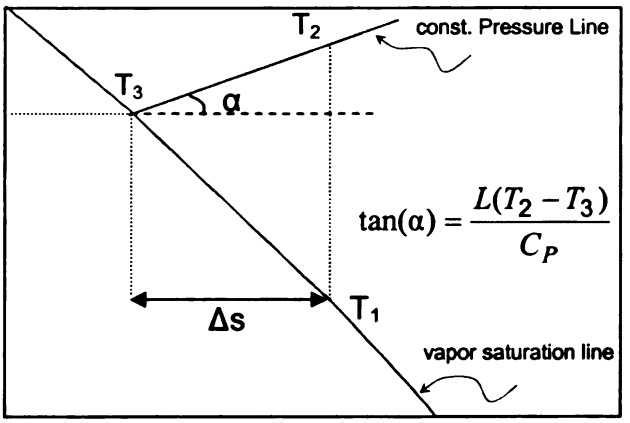

Figure 10: Slope of a constant pressure line in Temperature-Entropy diagram

The numerator of equation (13 is the logarithmic average between temperatures T_2 to T_3. Therefore,

$$\tan(\alpha) = \frac{L(T_2 - T_3)}{C_P} \tag{14}$$

Equation 14 shows the slope of constant pressure lines leaving the saturation area to the superheated region for any refrigerant. Therefore, for a constant temperature change from T_2 to T_3, the slope of constant pressure lines are inversely related to Cp average between the two temperatures. Also, Δs for each refrigerant determines the slope of saturated vapor line for a constant temperature lift. For the purpose of comparison, a parameter Λ_{lift} has been introduced as

$$\Lambda_{lift} = \frac{\Delta s}{(C_p)_{ave}} \tag{15}$$

Λ_{lift} is a factor for desuperheating irreversibility comparison of different refrigerants at a constant temperature lift. The higher the desuperheating

factor Λ_{lift}, the higher the desuperheating irreversibility associated with that refrigerant is.

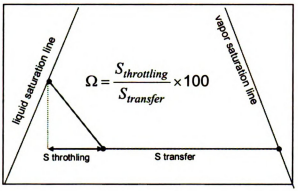

Figure 11: Throttling irreversibility factor in a T-s diagram

During the throttling process, however, any change in entropy is identified as irreversibility of the throttling process. As shown in Figure 11, the amount of irreversibility has to be compared to the entropy transfer during the evaporation process. For this reason, the throttling irreversibility factor Ω is defined as

$$\Omega = \frac{S_{throttling}}{S_{transfer}} \times 100 \tag{16}$$

So, the higher the Ω factor the higher the throttling irreversibility associated with a specific refrigerant.

Refrigerant	R22	R290	R717	R134a	R123	R718
Λ	0.046	0.01	0.12	0.01	0	0.36
Ω	5.11	2.94	0.76	5.53	5.64	0.26

Table 2: Comparison of irreversibility and throttling factors for several refrigerants for $T_{evap.}$=5°C and $T_{cond.}$=35°C

Table 2 shows Λ_{lift} and Ω factor for some selected refrigerants for a 30°C temperature lift. As shown, water has the most desuperheating irreversibility among the investigated refrigerants. On the other hand, R718 has the least throttling irreversibility. This interesting fact shows that any improvement in the compression process will significantly improve the efficiency of R718 cycles. A simple theoretical calculation shows when R718 is used in multistage compressors with intercooling, it achieves a significant COP increase.

Table 2 shows the desuperheating factor of 0 for R123. The reason is that R123 vapor saturation line has positive inclination. Therefore, when a refrigerant leaves the evaporator and, in ideal case, expands isentropically, it still will be inside the T-s dome. Therefore, there will be no desuperheating irreversibility for this refrigerant.

2.3. COMPARISON IN A PRESSURE ENTHALPY DIAGRAM

One challenge when using water as a refrigerant is that for common refrigeration conditions water has to work under vacuum. Figure 12 compares water to the two most common refrigerants, R134a and R717 (ammonia), in a log pressure- enthalpy diagram. In this figure, an operating condition of 5 °C evaporation temperature and 30 °C temperature lift is considered. It is noticeable that R718 cycle is operating in less than 1 atm pressure. Also, the enthalpy change during evaporation for R718 is much more compared to the other two.

Although the specific enthalpy of R718 during evaporation is highest of all among investigated refrigerants, its volume flow is still the highest. To compare

volume flow of investigated refrigerants, a non conventional T-Δh/v is shown in Figure 13.

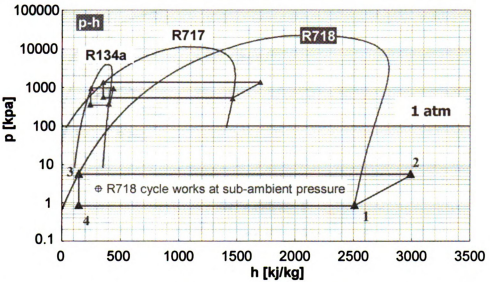

Figure 12: Log pressure-Enthalpy diagram for R718, R717, and R134a

Based on Figure 13, R718 has the least cooling capacity per volume. In another word, R718 has the highest specific volume flow, i.e. the volume of the flow that must be compressed to obtain a unit cooling capacity.

Table 3 compares common refrigerants for a fixed typical evaporation and condensation temperature. Among all, water requires the highest pressure ratio for a fixed temperature lift, which results in a high temperature discharge for the compressor. Therefore, in refrigeration cycles working with water as a refrigerant, a multistage compressor is used with intercooling.

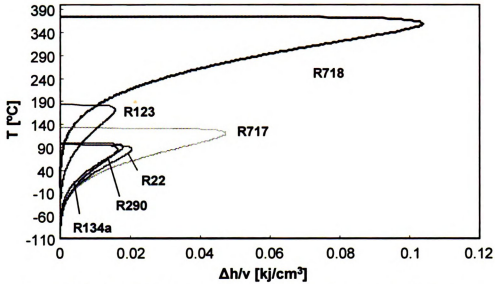

Figure 13: Temperature-Enthalpy per specific volume diagram

Quantity	R718	R134a	R717	R290	R22	R123
Evap. Temp [°C]	5					
Cond. Temp [°C]	35					
Comp. Temp [°C]	257 two-stage 178 one-stage	46	99	45	60	46
Specific Volume [m^3/kg]	147	0.008	0.002	0.002	0.0008	0.0006
Mass Flow Rate 100 ton [kg/s]	0.15	2.20	0.31	1.74	2.05	2.28
Compression Ratio*	6.4	2.5	2.6	2.2	2.3	3.2
Pressure Lift [Kpa]	4.75	537	835	667	545	897
COP Carnot	9.27					
COP**	5.01 one-stage 5.54 two-stage	5.50	5.46	5.42	5.45	5.70

*Two-stage calculations are based on perfect intercooling and the same pressure ratio for each stage.

** COP calculations are for the same polytrophic efficiency of 0.7.

Table 3: Comparison of different refrigerants in a typical evaporation and condensation temperature

As shown in this table, when water is used with multistage compressors, its COP is competitive to common refrigerants. Also, because compression part is the key

for improving refrigeration cycles working with water, any cycle modification leading the use of innovative cycles or compressors will result in better performance of water compare to other investigated refrigerants.

2.4. COEFFICIENT OF PERFORMANCE COMPARISON

2.4.1 COMPARING COP OF WATER (R718) AND R134a

R134a is a very attractive refrigerant with zero ozone depletion and is the refrigerant of choice in automotive air-conditioning. As shown in Figure 12, the disadvantage of R134a compare to other refrigerants is the low specific refrigerating capacity.

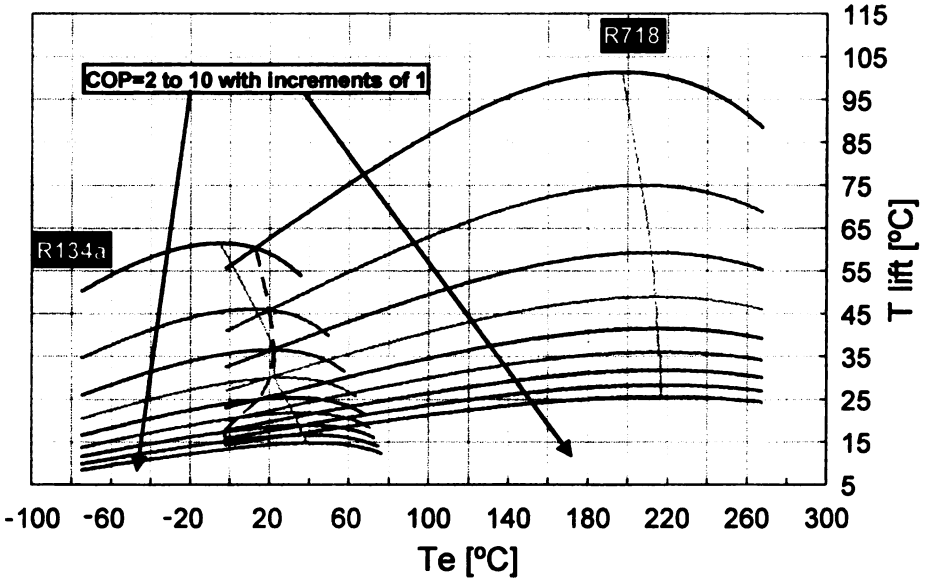

Figure 14: COP isolines for R718 and R134a refrigerants

Figure 14 shows the constant COP lines of water and R134a. In this graph, the abscissa is the evaporation temperature and the ordinate is the temperature lift. In this comparison, the same polytropic efficiency is considered (assumed 0.7). The use of a polytropic rather than isentropic compression efficiency

ensures that the overall performance of the compression process was not influenced by the number of compression stages. Also, in these graphs the effect of heat exchangers is reflected by moving the graphs of R134a and R718 diagonally to the origin. The background comes from the benefit of using direct heat exchangers in the case of R718. For water in most cases, an internally direct heat exchangers with 1°C temperature difference plus external plate heat exchangers with 1°C difference (equal to 2°C) are used. Whereas with R134a, normally 5°C can be assumed for internal indirect heat exchangers. This gives 2°C or 5°C respectively for R718 and R134a for the evaporator (T_e) and again 2°C or 5°C respectively for R718 and R134a for the condenser (T_{lift}). In this graph no subcooling or superheating is considered for R718. For R134a, 10°C superheating and 5°C subcooling is considered (Table 4 and [27]).

	R718	R134a
min temp. difference evaporator [k]	1	5
min temp. difference condenser [k]	1	5
min temp. difference plate heat exchanger [k]	1	-
Overheating [K]	-	10
Undercooling [K]	-	5

Table 4: Marginal conditions for the performance comparison in Figure 14, taken from Ref. [27]

In Figure 14 the maximum of each COP isoline is connected with a solid yellow line. This line represents the best operating point for each refrigerant. From this line it is evident that, in the case of water, the higher the evaporation temperature, the higher COP for a fixed temperature lift will be. In this graph the

intersection of same isolines are connected with a dashed green line. This line represents that for any evaporation temperature to the right of this line, the choice of water as a refrigerant with a fixed temperature lift will result in a better COP. The graph also shows that for relatively high temperature lift (greater than 60K) choice of water as a refrigerant represents better COPs.

2.4.2. COMPARING COP OF WATER (R718) AND AMMONIA (R717)

Ammonia is an excellent refrigerant with a high latent heat and excellent heat transfer characteristics. However, because of its toxicity, it is often restricted to applications in which the equipment is outdoors to allow natural dilution of any leaks.

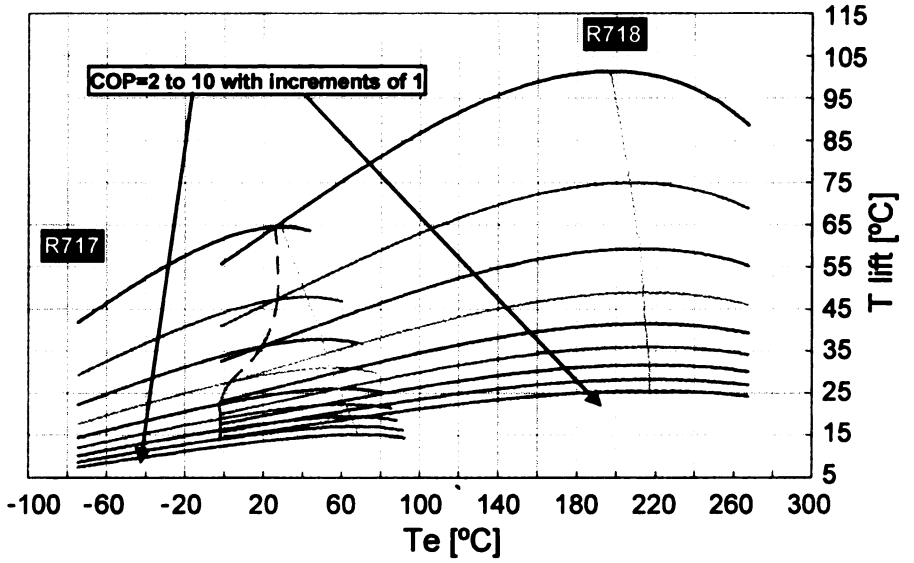

Figure 15: COP isolines for R718 and R717 refrigerants

Figure 15 shows the constant COP lines of water and ammonia. In this graph, the abscissa is the evaporation temperature and the ordinate is the temperature lift. In this comparison, like the pervious one, the same polytropic efficiency is

considered (assumed 0.7). In these graphs the effect of heat exchangers are reflected as described in the pervious comparison. In this graph, the solid line connecting the maximum of COP isolines of ammonia covers a wider evaporation temperature range than that of R134a. However, in this case for low evaporation temperatures and low temperature lifts water performs better in terms of COP.

CHAPTER 3: IMPLEMENTATION OF A CONDENSING WAVE ROTOR

3.1. WAVE DEVICES

A gas in a supersonic flow can be compresses in three methods: Isentropic, Prandtl-Meyer, and shockwave. The method of compression of a gas results in different temperatures and densities for a given pressure ratio, which can be analytically calculated for a non-reacting gas. A shock wave compression results in a loss of total enthalpy, meaning that it is a less efficient method of compressing gases for some purposes, for instance in the intake of a scramjet. However, by generating shock waves in appropriate geometries, unsteady wave machines can transfer the energy of a high-pressure fluid directly to another low-pressure fluid without using mechanical components, such as pistons or vaned impellers. This is one of the reasons that the potential for using wave devices in thermodynamic cycles for power generation, propulsion, and refrigeration has attracted the attention of researchers since the early twentieth century. Shock tubes, shock tunnels, pressure exchangers, pulse combustors, pulse detonation engines, and wave rotors are among the best-known wave devices developed thus far. These devices represent applications of classical nonsteady, one-dimensional compressible flow theory. It is well known, but not yet widely employed, that time-dependent flow devices can generate much greater pressure rises than those obtained in steady-state flow devices [40-42].

Within the family of wave devices, wave rotors have demonstrated a favorable potential for reaching the ultrahigh performance targets of power systems and for lowering their cost. A wave rotor is a dynamic pressure

exchanger that exchanges energy from a high pressure fluid to a low pressure fluid via the means of moving shock waves that are generated in an appropriate geometry by exposing the ends of flow channels alternatively to high pressure and low pressure ports (Figure 16).

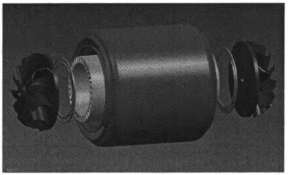

Figure 16: Schematic configuration of a typical wave machine [43]

Much research has been devoted to the progress and development of wave rotor technology, especially in the past few decades. Most of the work in the U.S. expands from the early efforts of the General Electric Company (GE), General Power Corporation (GPC), and Rolls Royce [44,45] to the recent activities of the wave rotor team at NASA Glenn Research Center (GRC) collaborated by the U.S. Army Research Laboratory (ARL) and Rolls-Royce Allison [46-55].

In recent years, Turbomachinery Laboratory of Michigan State University has been actively pursuing research in different propulsion and power generation purposes. Research teams at Warsaw University of Technology in Poland, Purdue School of Engineering and Technology in Indianapolis (IUPUI), and University of Tokyo are other examples of active research in the area of unsteady wave devices, specifically the wave rotors [56].

3.2. WAVE ROTOR

Utilization of unsteady flow devices to enhance the performance of thermodynamic cycles has been a major branch of study since the early twentieth century. The basic concept underlying these devices is the transfer of energy with shock waves. By generating compression waves in appropriate geometries, unsteady wave machines can transfer the energy of a high-pressure fluid directly to another low-pressure fluid. Thus, a pressure rise can be obtained without using mechanical components such as pistons or vaned impellers. [57].

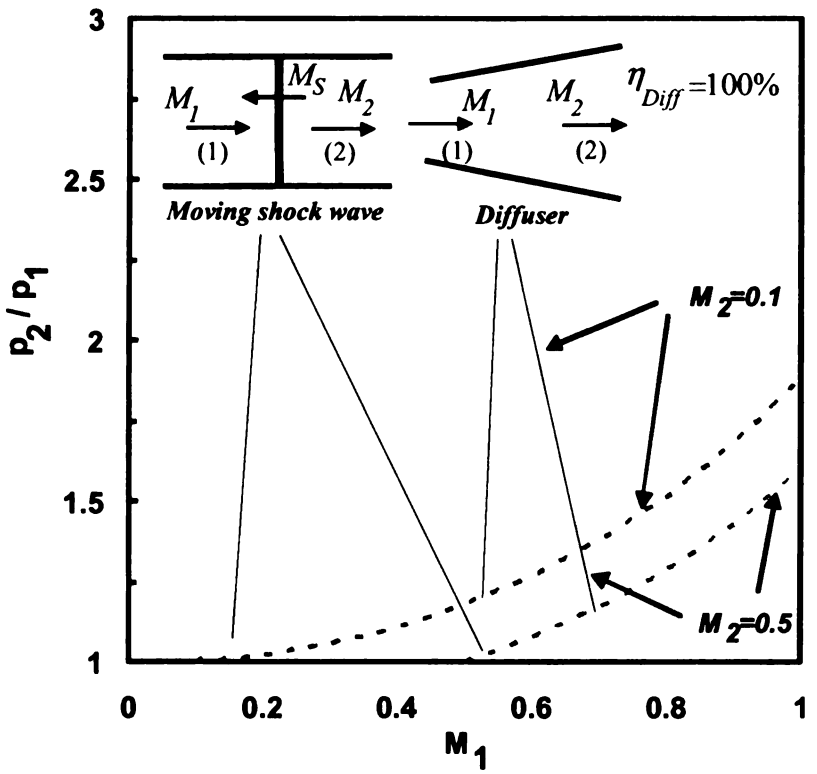

Figure 17: Comparison of pressure gain (static pressure ratio) of moving shock and steady flow isentropic diffuser for γ=1.4 [42]

For instance as shown in Figure 17, for the same change from a given inlet Mach number M_1 to a given outlet Mach number M_2, the static pressure ratio p_2/p_1 across a single shock wave moving in a frictionless channel (solid line) is always much greater than that obtained by an isentropic deceleration in a 100%

efficient diffuser (doted line). However, it must be noted that friction effects always exist, and hence pressure gains are actually less than those predicted by Figure 17. It is also useful to compare the shock wave isentropic efficiency (η_{Shock}) with the diffuser efficiency (η_{Diff}). Figure 18 shows variations of η_{Shock} (solid line) and η_{Diff} (dashed line) as functions of the pressure gain p_2/p_1 obtained by a moving shock wave in a frictionless channel and by a diffuser, respectively. η_{Diff} is calculated for different values of total pressure drop across the diffuser expressed by p_{t2}/p_{t1}. Similar flow friction-effects would lower the efficiency of wave devices and reduces the efficiency advantage of such devices, which is not shown in Figure 18 [42].

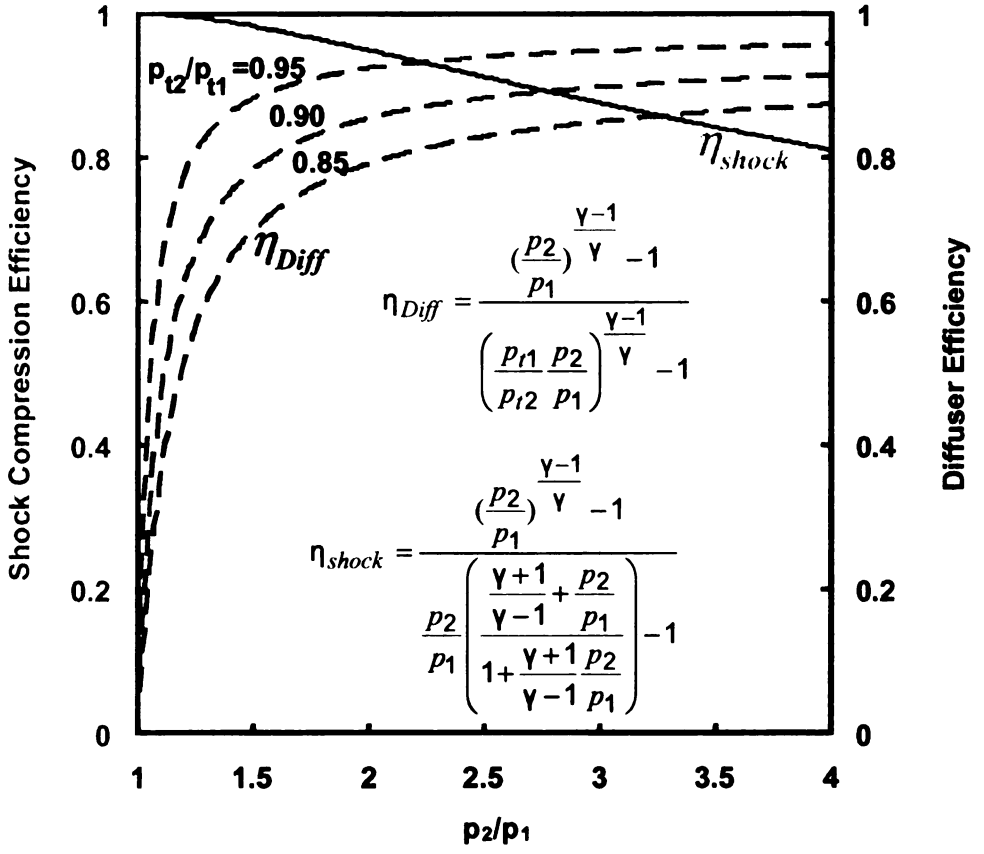

Figure 18: Shock wave and diffuser isentropic efficiencies as a function of the static pressure ratio [42]

The comparison in Figure 18 reveals that for the same pressure gain p_2/p_1, shock compression efficiency may far exceed the efficiency obtained by a diffuser. Thus, it is seen that for a pressure recovery of up to p_2/p_1=2.2, η_{Shock} is greater about 93% and hence it is always greater than that of a usual diffuser. Therefore, by substituting a diffuser with an unsteady flow device utilizing shock waves, a gain in cycle performance can be expected.

There are at least two classes of wave machines: rotating wave machines and non rotating wave machines. Dynamic pressure exchangers and wave rotors are two types of rotating wave devices developed to reach the high performance targets of thermodynamic cycles. In Europe, however, both terms were often used interchangeably [58]. The first available literature on dynamic pressure exchangers utilizing pressure waves is a patent in 1929 filed by Burghard [59]. This patent has introduced the concept of the dynamic pressure exchanger. The essential feature of these devices is an array of several channels arranged around the axis of a cylindrical rotor. The assembly rotates between two end plates, each of which has a few ports or manifolds that control the fluid flow through the channels. Through rotation, the channel ends are periodically exposed to the steady state ports located on the end plates causing the initiation of compression and expansion waves within the passages. Therefore, unlike a steady-flow turbomachine component, which either compresses or expands the gas, both compression and expansion are accomplished within a single component. A reversed design with stationary rotor and rotating ports is also possible [60]. Such a configuration may be preferred for laboratory investigations

because it easily enables flow measurement in the channels where the important dynamic interactions take place. However, this arrangement rarely seems to be convenient for commercial purposes [61].

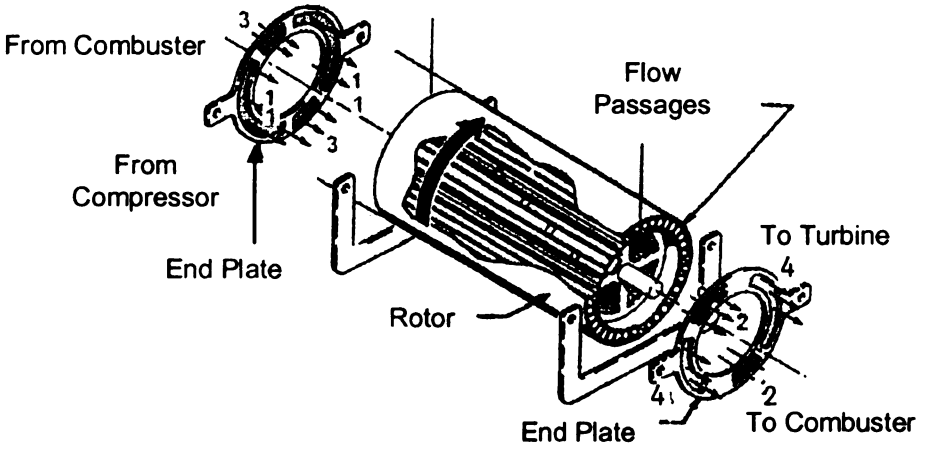

Figure 19: Schematic configuration of a typical wave machine

Figure 19 schematically represents most of the rotating wave devices. Each end plate contains a few ports. To minimize leakage, in practice, there is only a very small gap between the end plates and the rotor and the end plates with sealing material may contact the rotor. The rotor may be gear or belt driven [61] or preferably direct driven by an electrical motor (not shown in the picture). The power required to keep the rotor at a correctly designed speed is very small, it is almost zero [62]. It is just an amount necessary to overcome rotor windage and the friction in the bearing and contact sealing if used. Alternatively, rotors can be made self-driving. This configuration called the "free running rotor" can drive itself by angling the blades against the direction of rotation [63]. In this case, the momentum of the inflow or outflow rotates the rotor.

In dynamic pressure exchanger and wave rotors two basic fluid-exchange processes usually happen at least once per revolution of the rotor: the high

pressure process (charging process) and the low pressure process (scavenge process). In the high pressure process, compression waves transfer the energy directly from a fluid at a higher pressure to another fluid at a lower pressure. The low pressure process employs expansion waves to scavenge the flow from the rotor channels. Ingestion of the fresh cold fluid into the rotor channels is also performed in this process [42].

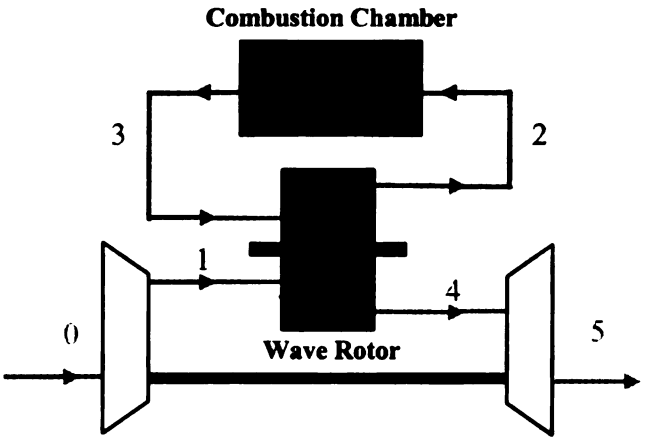

Figure 20: A schematic of a gas turbine topped by a 4-port wave rotor [42]

Advantageous of using wave rotor can be summarized as:

- Potentially have higher efficiency than turbomachines
- Higher overall engine pressure ratio
- More compact systems as they combine compressor and turbine stage in one device
- Lower rotational speed compared to turbomachines, which results in low material stresses
- Simpler design and geometry compare to turbomachines. Therefore, lower manufacturing costs.

- Channels are less prone to erosion damage than the blades of turbomachines. This is mainly because of the lower velocity of the working fluid in the channels, which is about one-third of values within turbomachines [61].
- Self-cooling capabilities. Wave rotors are naturally cooled by the fresh cold fluid ingested by the rotor. Therefore, applied to a heat engine, the rotor channels pass through cool air and high-pressure and high-temperature gas flow in each rotor revolution. Therefore, the rotor material temperature is always maintained between the temperature of the cool air which is being compressed and the hot gas which is being expanded.

3.3. APPLICATION OF WAVE DEVICES IN REFRIGERATION CYCLES

As discussed above, refrigeration cycles working with water as a refrigerant require bulky multistage compressors; therefore, making them not suitable for small scale applications such as home size refrigeration. On the other hand, application of wave rotors in the gas turbine cycles and their significant energy savings introduce a potential application in cycles involving phase change.

Increasing the pressure difference in liquid state requires a simple pump; however, when the substance is in vapor phase, a high technology compressor is required to provide a high pressure ratio. Therefore, for instance, in the R718 cycle, if we could provide a portion of pressure ratio required in vapor phase in the liquid state, the size and the cost should decrease.

Base on the above idea and ongoing research on wave devices and refrigeration cycles at Michigan State University, a novel idea of Condensing Wave Rotor sparked which later, lead to a US patent application by Norbert Mueller.

Adding a wave rotor to a R718 cycle enables greater temperature lift or reduces the compressor pressure ratio, which is crucial for the R718 chiller technology, where the stage pressure ratio is very much limited by the thermodynamic properties of water vapor. Although invention of Condensing Wave Rotor was started in R718 cycles, its application can be investigated for other refrigeration cycles or, even beyond that, any cycle involving phase change and compression of a gas.

The present study demonstrates the enhancement of a turbocompression refrigeration cycle that uses water as refrigerant (R718) by utilizing a novel 3-port condensing wave rotor. This device is meant to be designed such that its existence in the cycle compensates for one stage of compressor. At the same time, the condensation of the refrigerant occurs inside its channels. Therefore, overall size of the refrigeration equipment is expected to be reduced significantly.

In the following chapters, beside investigation of R718 cycles and wave rotors, a detailed study of condensing wave rotors, and its design, and analytical study is presented.

3.4. CONDENSING WAVE ROTOR

The novel idea of condensing wave rotor springs from extensive research for implementation of conventional wave rotor in gas turbines. Wave rotors appear in

different configurations and different number of inlet and outlet ports. As described in previous chapters, in R718 refrigeration cycles, the key component is the compressor. To achieve better COPs and smaller R718 units, one solution could be implementation of a wave rotor in R718 units. For this purpose, a 3-port wave rotor is considered. Concerning the pressure levels, 3-port wave rotors' function is similar to pressure-equalizers' [61] like the one depicted in Figure 21.

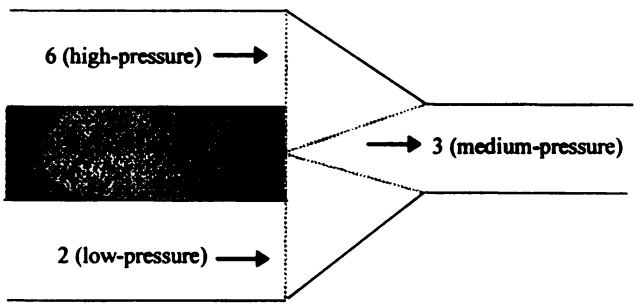

Figure 21: Dynamic-pressure equalizer

The phase change of the fluid inside the wave rotor in a R718 refrigeration application is a major difference to the operation of a wave rotor in a gas turbine cycle. Additionally, here the low pressure fluid is at higher temperature than the high pressure fluid. In this innovative design, condensation of vapor occurs inside the wave rotor; therefore, it is called condensing wave rotor. A schematic of a 3-port condensing wave rotor is depicted in Figure 22. The condensing wave rotor provides energy exchange in liquid state which is much more economical and easier than vapor phase. The liquid leaving the device is pumped to a higher pressure level, and then, is introduced suddenly to a low pressure vapor phase in the channels. The details of process are discussed in future chapters.

R718 cycle is the first application researched for condensing wave rotor. This novel idea has a potential to be implemented in any application with phase change, where providing the required pressure ratio is difficult. Also, water is the first refrigerant researched for condensing wave rotor fluid. Condensing wave rotor has the potential of being used on other refrigeration cycles such as CO_2 refrigeration cycles or even R134a.

Simply, because of the novelty of the condensing wave rotor, the author only focuses on application of condensing wave rotors in the refrigeration cycles, and only for refrigeration cycles using water as a refrigerant.

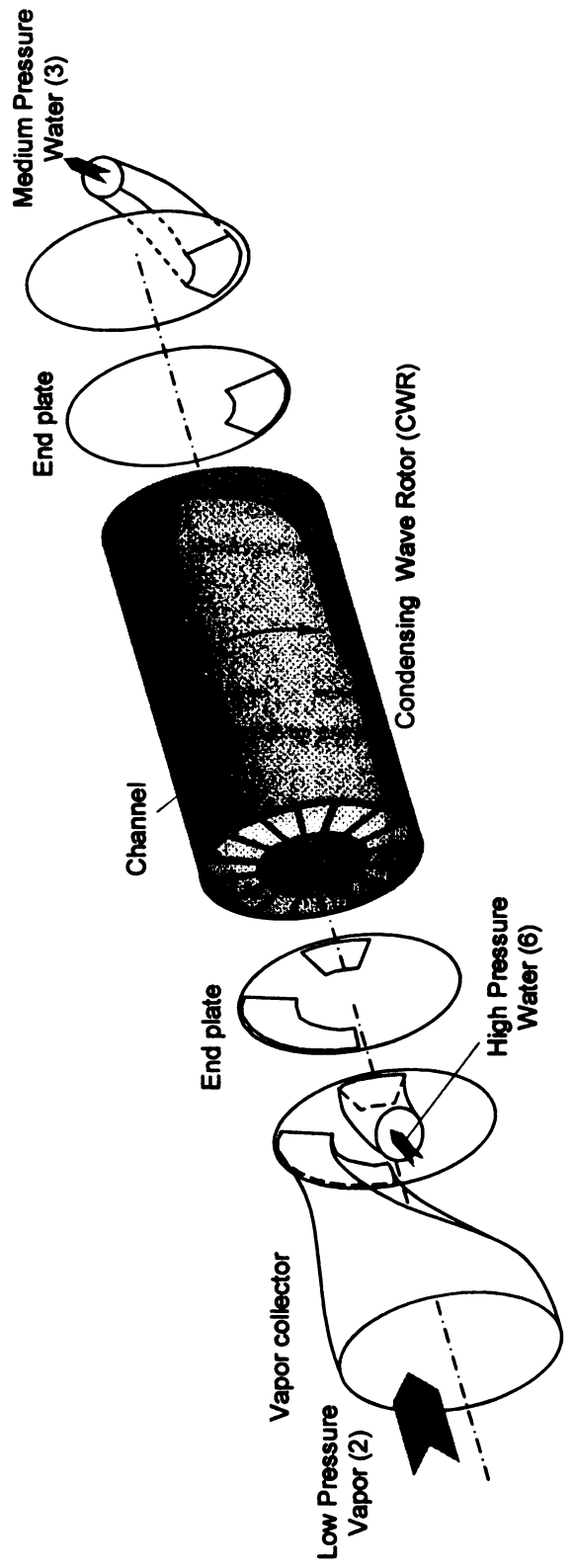

Figure 22: Schematic of a 3-port condensing wave rotor

CHAPTER 4: ANALYSIS OF CONDENSING WAVE ROTORS

4.1. INTERNAL: TRANSPORT AND PHASE CHANGE PHENOMENA

A schematic thermodynamic model of a R718 cycle using a 3-port condensing wave rotor is depicted in Figure 23.

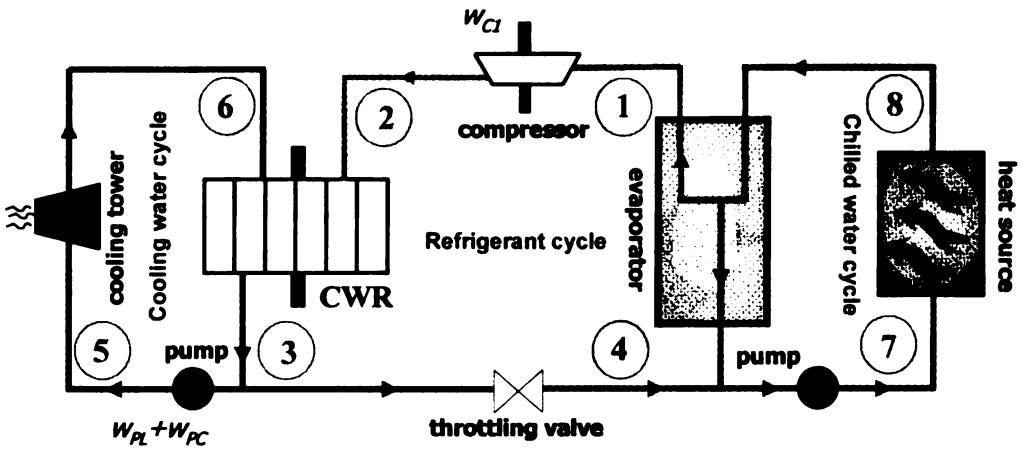

Figure 23: Schematic of the thermodynamic model of a R718 chiller unit enhanced by a 3-port condensing wave rotor (CWR) substituting for the condenser and for one stage of compressor

While Figure 22 shows a schematic of a 3-port condensing wave rotor, Figure 24 schematically shows the regions modeled for a channel during compression and condensation. The following explanation follows the points (states) introduced in Figure 23. Coming from the turbocompressor (2), the superheated vapor flows continuously through a vapor collector (shown in Figure 22) to the inlet port of the wave rotor located at one of the two stationary end plates. By rotating the wave rotor between the two end plates, the wave rotor channels are opened to the port and filled with the incoming superheated vapor.

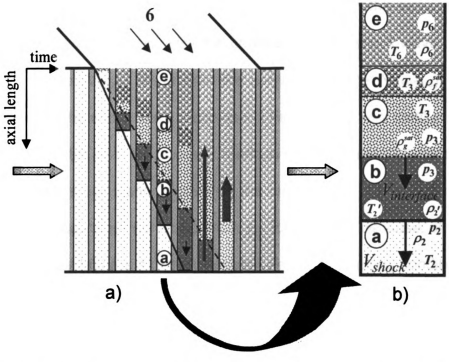

Figure 24: a) Schematic wave and phase-change diagram for the 3-port condensing wave rotor (high-pressure part) b) A magnified channel showing the regions modeled during compression and condensation.

Region (*a*) in Figure 24 is the state after the filling process is completed. After further rotation, the channels meet the second-inlet port (6) through which the high-pressure low-temperature water (*e*) comes in and is exposed to the low-pressure high-temperature superheated vapor in region (a). Because of the sudden pressure drop (from p_6 to p_2), all the heat cannot be contained in the incoming water as sensible heat and the heat surplus is transformed into latent heat of vaporization. This is the so-called flash evaporation or flashing phenomenon [57, 65]. Therefore, one portion of the incoming water suddenly vaporizes (*c*) and the remaining part cools down (*d*). The frontal area of the saturated vapor (c) generated by the flash evaporation is called the contact interface and acts like a fast-moving piston. It causes a shock wave triggered

from the leading edge of the inlet port traveling through the superheated low-pressure vapor, which exists inside the channel (*a*). The shock wave travels with supersonic speed (V_{shock}) faster than the contact interface ($V_{interface}$). Therefore, the trajectory of the shock wave (solid line in Figure 24) has a smaller slope than the incoming water and the contact interface of the generated vapor (dashed line). Behind the moving shock wave (*b*) the temperature is increased from T_2 to $T_{2'}$ and the pressure is increased from p_2 to $p_{2'} = p_3$ because of the shock compression. The latter is a design decision similar to a tuning condition. With it, the pressure at the inlet port p_6 is set to an appropriate value that generates the pressure ratio p_6/p_2 required to trigger the desired shock wave. The superheated vapor will be condensed at pressure p_3 . This shows that the fluid in its liquid state serves as a "work capacitor" storing pump work to release it during its expansion in the wave rotor channels for the simultaneous vapor compression. Therefore, in the enhanced system the pump in the cooling water cycle not only has to provide the work necessary to overcome the pressure loss in the heat rejecter cycle w_{PL}, but also the work necessary for the shock wave compression in the wave rotor channels w_{PC}. The pressure behind the shock wave (*b*) is imposed on the vapor generated by the flash evaporation (*c*). It is the pressure at the water surface and the equilibrium pressure at which the evaporation decays $p(c) = p(b) = p_3$. Hence, both generated vapor and the cooled water obtain the saturation temperature $T_3 = T_{sat}(p_3)$.

Because of the direct contact of the superheated compressed vapor (*b*) with the cold incoming water (*e*), the superheated vapor is desuperheated and its heat

is transferred (*f*) to the incoming water. This continues until the equilibrium temperature T_3 is achieved in region (*b*) and the superheated vapor is changed to saturated vapor. Subsequently, the incoming water compresses the saturated vapor further and condenses it, while the latent heat is transferred to the incoming water (*g*). The water, which is nearly a fully condensed two-phase vapor with a typical quality of 0.005, is scavenged through the only outlet of the wave rotor (3). The scavenging process may be supported by gravity and pump power.

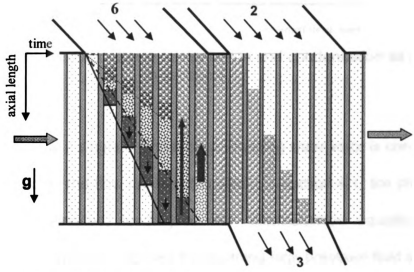

Figure 25: Schematic wave and phase-change diagram for the 3-port condensing wave rotor including the discharge process

Figure 25 shows the discharge process for a design of condensing wave rotor. In this design, the only outlet port in opened exactly at the same time as the low pressure port is opened. Therefore, column of water will flow downward because of gravitational force to the water mass inside the channel and low pressure water vapor coming from compressor takes the emptied space. The

outlet port is kept opened until the liquid water is fully scavenged. Then, the cycle repeats.

4.1.1 STUDY OF FLOW INSIDE A CHANNEL OF A CONDENSING WAVE ROTOR

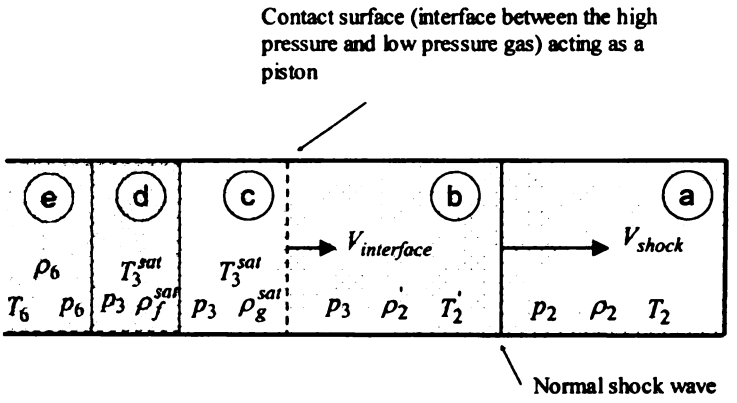

Figure 26: Regions modeled during compression and condensation as described in section 4.1

For simplicity, only a single channel of condensing wave rotor is considered in this section. Based on the flow regimes described in section 4.1, the shock wave calculations are presented, leading to the "characteristic equation", which determines the inlet pressure required for incoming high pressure fluid so that the outlet fluid is saturated liquid in a prescribed outlet pressure.

4.1.1.1. TEMPERATURE INCREASE ACROSS THE NORMAL SHOCK WAVE

Consider p_3, T_2, and p_2 are known variables, and $T_{2'}$ is a known variable. p_3 is the outlet pressure of the condensing wave rotor. T_2 and p_2 are the temperature and the pressure of the low pressure port; on the word, the outlet state of the compressor.

Defining the Mach number as

$$M = \frac{V_{shock}}{a_2} \tag{17}$$

where a_2 is the speed of sound in region *a*, the Mach number is related to the pressure ratio across the wave [67]

$$\frac{p_3}{p_2} = \frac{2\gamma}{\gamma+1}(M^2 - 1) + 1 \tag{18}$$

From equation 18

$$M = \sqrt{\frac{\gamma+1}{2\gamma}(\frac{p_3}{p_2} - 1) + 1} \tag{19}$$

The relationship between the temperatures across a normal shock is [67]

$$\frac{T_2'}{T_2} = \frac{(1 + \frac{\gamma-1}{2}M^2)(\frac{2\gamma}{\gamma-1}M^2 - 1)}{\frac{(\gamma+1)^2}{2(\gamma-1)}M^2} \tag{20}$$

where T_2' is the temperature in region *b* and can be determined as

$$T_2' = T_2 \frac{(1 + \frac{\gamma-1}{2}M^2)(\frac{2\gamma}{\gamma-1}M^2 - 1)}{\frac{(\gamma+1)^2}{2(\gamma-1)}M^2} \tag{21}$$

Using equation 19 and 21, the following equation is derived

$$T_2' = T_2 \frac{\left(1+\frac{\gamma-1}{2}\left[\frac{\gamma+1}{2\gamma}\left(\frac{p_3}{p_2}-1\right)+1\right]\right)\left(\frac{2\gamma}{\gamma-1}\left[\frac{\gamma+1}{2\gamma}\left(\frac{p_3}{p_2}-1\right)+1\right]-1\right)}{\frac{(\gamma+1)^2}{2(\gamma-1)}\left[\frac{\gamma+1}{2\gamma}\left(\frac{p_3}{p_2}-1\right)+1\right]} \tag{22}$$

Equation 22 shows that by knowing the pressure of outlet p_3, temperature T_2, and pressure p_2 of low pressure inlet, the temperature in region *(b)* T_2' can be obtained.

4.1.1.2. INTERFACE VELOCITY ACROSS THE NORMAL SHOCK WAVE

Again, p_3, T_2, and p_2 are known variables. The following derivation is to calculate the the interface velocity $V_{interface}$ across the normal shock wave.

The relationship for the density across a normal shock wave is [67]

$$\frac{\rho_2'}{\rho_2} = \frac{\gamma+1}{2}\left(\frac{M^2}{1+\frac{\gamma-1}{2}M^2}\right) \tag{23}$$

Substituting equation 19 in the above equation gives

$$\frac{\rho_2'}{\rho_2} = \frac{\gamma+1}{2}\left(\frac{\left[\frac{\gamma+1}{2\gamma}\left(\frac{p_3}{p_2}-1\right)+1\right]}{1+\frac{\gamma-1}{2}\left[\frac{\gamma+1}{2\gamma}\left(\frac{p_3}{p_2}-1\right)+1\right]}\right) \tag{24}$$

or

$$\frac{\rho_2'}{\rho_2} = \frac{1+\left(\frac{\gamma+1}{\gamma-1}\right)\frac{p_3}{p_2}}{\frac{\gamma+1}{\gamma-1}+\frac{p_3}{p_2}} \tag{25}$$

Assuming V_2 is zero (low pressure vapor is stagnant when reaching the high pressure port), the continuity equation between regions *a* and *b* is

$$\rho_2 V_{shock} = \rho_2'(V_{shock} - V_{interface}) \tag{26}$$

Therefore,

$$\frac{\rho_2'}{\rho_2} = \frac{V_{shock}}{V_{shock} - V_{interface}} = \frac{M}{M - \frac{V_{interface}}{a_2}} \tag{27}$$

from which $V_{interface}/a_2$ is determined as

$$\frac{V_{interface}}{a_2} = M(1 - \frac{\rho_2}{\rho_2'}) \tag{28}$$

Now, applying equation 19 and equation 24 to the above equation gives

$$\frac{V_{interface}}{a_2} = \sqrt{\frac{\gamma+1}{2\gamma}(\frac{p_3}{p_2} - 1) + 1}\left(1 - \frac{\frac{\gamma+1}{\gamma-1} + \frac{p_3}{p_2}}{1 + (\frac{\gamma+1}{\gamma-1})\frac{p_3}{p_2}}\right) \tag{29}$$

or

$$\frac{V_{interface}}{a_2} = \sqrt{\frac{\gamma+1}{2\gamma}\frac{p_3}{p_2} + \frac{\gamma-1}{2\gamma}}\frac{2(\frac{p_3}{p_2} - 1)}{(\gamma+1)\frac{p_3}{p_2} + (\gamma-1)} \tag{30}$$

or

$$\frac{V_{interface}}{a_2} = \frac{1}{\sqrt{\gamma}}(\frac{p_3}{p_2} - 1)(\frac{2}{(\gamma+1)\frac{p_3}{p_2} + (\gamma-1)})^{0.5} \tag{31}$$

Speed of sound in region *a* is $a_2 = \sqrt{\gamma.R.T_2}$; therefore,

$$V_{interface} = (\frac{p_3}{p_2} - 1)(\frac{2RT_2}{(\gamma+1)\frac{p_3}{p_2} + (\gamma - 1)})^{0.5} \quad (32)$$

Therefore, knowing the pressure of outlet p_3, temperature T_2 and pressure p_2 of low-pressure inlet, the interface velocity $V_{interface}$ can be calculated.

4.1.1.3. CHARACTERISTIC EQUATION

The speed of interface equals the speed of incoming water V_L plus the speed of evaporation V_{ev}

$$V_{interface} = V_L + V_{ev} = \frac{\dot{m}_6}{\rho_6 A} + \frac{\dot{m}_{ev}}{\rho_3^{sat-g} A} \quad (33)$$

where ρ_g^{sat} is the density of region *c* and *A* is the cross sectional area of the channel. Saury [57] has introduced the flash evaporation rate coefficient *J* as

$$J = \frac{\dot{m}_{ev}}{A(p_6 - p_2)} \quad (34)$$

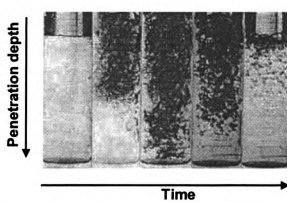

Figure 27: Flash evaporation photography by Miyatake [65]

Miyatake [65] has noted that J is not time dependent and has determined the value of J for several conditions. For other conditions J must be interpolated, extrapolated or determined through experiment. Thus, knowing J, $\dot{m}_{ev}$ can be obtained by

$$\dot{m}_{ev} = JA(p_6 - p_2) \tag{35}$$

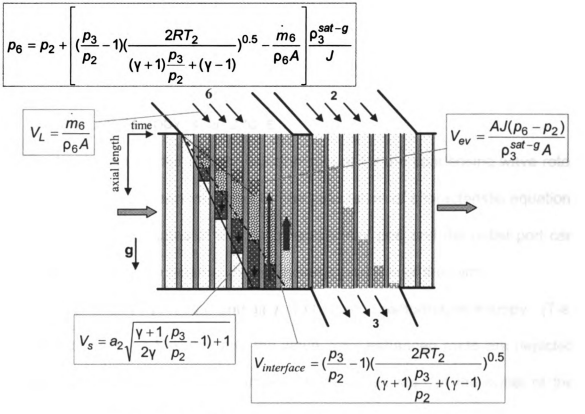

Figure 28: Condensing wave rotor wave diagram

; therefore,

$$\frac{\dot{m}_6}{\rho_6 A} + \frac{JA(p_6 - p_2)}{\rho_3^{sat-g} A} = \left(\frac{p_3}{p_2} - 1\right)\left(\frac{2RT_2}{(\gamma+1)\frac{p_3}{p_2} + (\gamma-1)}\right)^{0.5} \tag{36}$$

or solving for p_6

$$p_6 = p_2 + \left[\left(\frac{p_3}{p_2} - 1\right)\left(\frac{2RT_2}{(\gamma+1)\frac{p_3}{p_2} + (\gamma-1)}\right)^{0.5} - \frac{\dot{m}_6}{\rho_6 A} \right] \frac{\rho_3^{sat-g}}{J} \qquad (37)$$

The above equation is the characteristic equation of a condensing wave rotor. In the above equation knowing the exit temp T_3^{sat}, the density ρ_g^{sat-g} is known. Therefore, knowing the conditions of the gas inside the channel and the exit conditions, the high pressure port mass flow rate $\dot{m}_6$ may be a design factor for determination of its pressure p_6.

4.2. EXTERNAL: THERMODYNAMIC CYCLE

The low pressure inlet and the outlet pressure for the condensing wave rotor was considered as known variables for the calculation of characteristic equation. The thermodynamic states of the low pressure inlet port and the outlet port can be calculated using the external thermodynamic analysis of the cycle.

The schematic pressure-enthalpy (p-h) and temperature-entropy (T-s) diagrams of both the baseline and the wave–rotor-enhanced cycle are depicted in Figure 29 and Figure 30 respectively. Both cycles start at the outlet of the evaporator (state 1), where the vapor is saturated. State 2_b represents the compressor outlet of the baseline cycle, whereas state 2 is the compressor outlet of the wave-rotor-enhanced cycle, which allows using a compressor with a lower pressure ratio.

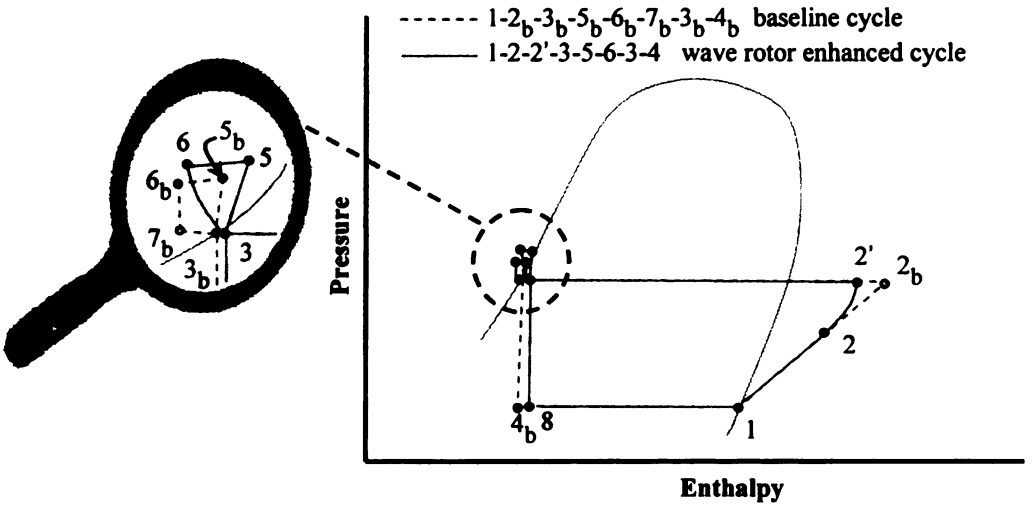

Figure 29: Schematic p-h diagram of a R718 baseline cycle and enhanced cycle with a 3-port condensing wave rotor.

State 2′ is an intermediate state inside the wave rotor channels that corresponds to the flow properties in region (*b*) right after the shock wave. The slope between states 2 and 2′ is greater than that between states 1 and 2_b because the shock compression typically occurs with a higher efficiency [40-42]. Still inside the wave rotor channel, the superheated vapor is desuperheated to the equilibrium temperature T_3 (2′→3). State 3 is actually much closer to the liquid region than shown in Figure 29 and Figure 30 because the mass flow rate of the cooling water cycle ($\dot{m}_6$) is much greater than that of the core cycle ($\dot{m}_2$). Knowing this, it becomes clear why the distances between states 3, 5, and 6 are magnified in this schematic diagram. The expansion process (6→3) releases the energy consumed by the compression process of the vapor (2→2′) all within the wave rotor channels.

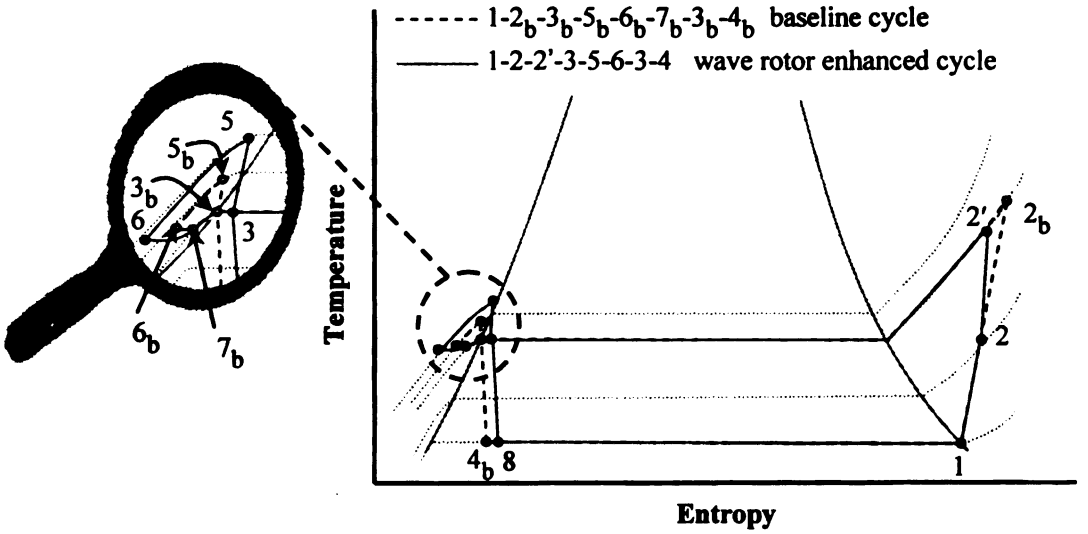

Figure 30: Schematic T-s diagram of a R718 baseline cycle and enhanced cycle with a 3-port condensing wave rotor

Coming from the only outlet port of the wave rotor (state 3), the flow diverges. The small fraction used as refrigerant is directed to the expansion valve and is expanded in a constant enthalpy process (3→4), while largest part of the flow out of the wave rotor is pumped (3→5), providing the energy for the vapor compression in the wave rotor w_{PC} and compensating for the pressure loss in the heat rejecter and associated piping w_{PL}. In this case, an inducer pump may be used to avoid cavitations problems. Then, the fluid goes into the heat rejecter (cooling-tower or similar) where it cools off (5→6). In the enhanced cycle, the inlet port of condensing wave rotor can be viewed as throttling; therefore, a separate expansion valve is not shown. In difference to the insenthalpic expansion (throttling), in the condensing wave rotor most of the pressure is recovered immediately for compression of the refrigerant gas in the channels of a condensing wave rotor. The expansion in the condensing wave rotor can be

viewed as a turbine expansion in which the work necessary for refrigerant compression is extracted.

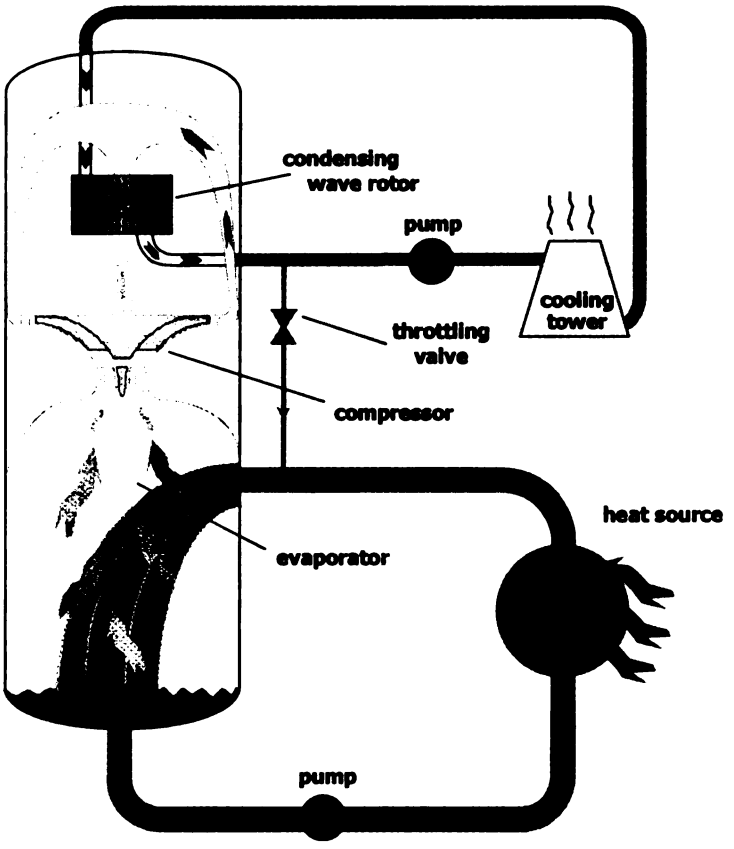

Figure 31: Novel compact R718 water chiller with integration of a condensing wave rotor

Figure 31 pictures one possible integration of a condensing wave rotor in a R718 cycle. This innovative design unifies a significant part of the compression with the desuperheating and condensation of the refrigerant vapor in a compact dynamic unit. Such innovative designs of R718 chillers with integration of condensing wave rotors will result in manufacturable, easily scalable (3-300 kW), and high-efficient refrigeration cycles.

4.3. SIZE COMPARISON

Using a 3-port condensing wave rotor in a water refrigeration cycle can improve the coefficient of performance of R718 units [64] while reducing their size and cost. Its successful implementation may replace three subsystems: the intercooler, one compressor stage, and the condenser. With conservative measures as shown in Figure 32, this may reduce the overall size of the R718 unit to nearly 50%, since the volume of these three subsystems reduces down to about one-tenth of the current size [27].

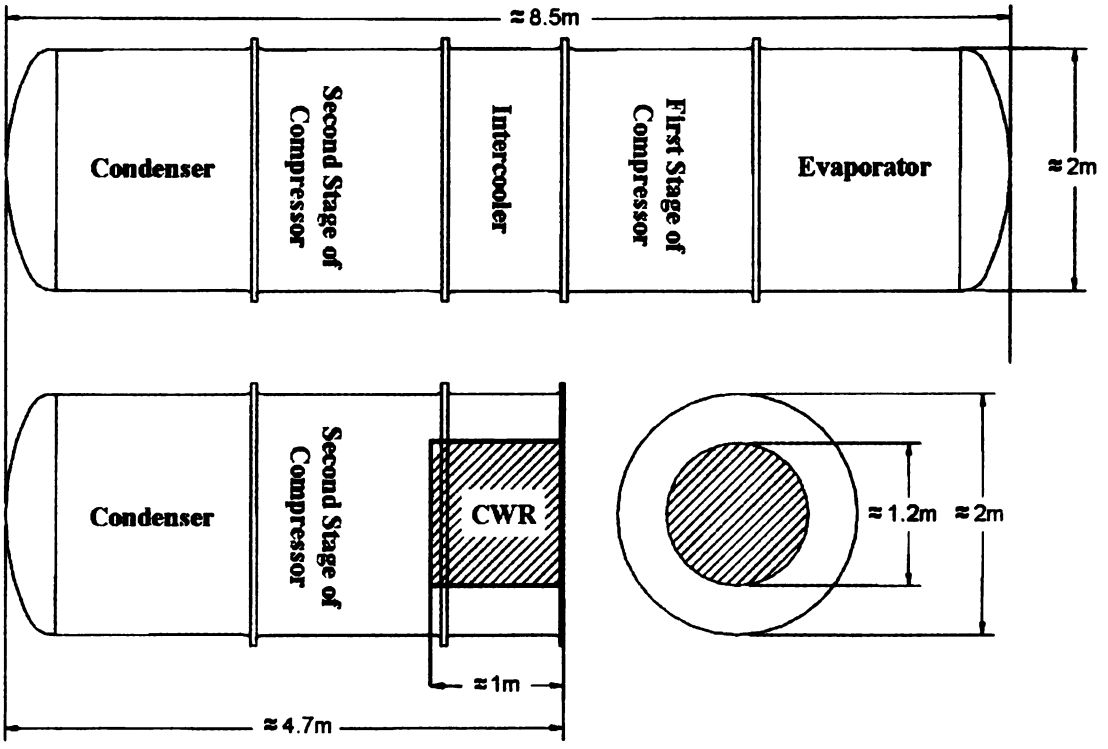

Figure 32: Size reduction by combining intercooler, second stage compression, and condensation into a condensing wave rotor (CWR)

It is noted that the wave rotor length is a design parameter that adjusts with rotational speed and the speed of sound within the fluid. The wave rotor diameter is governed by the volume flow rate of the precompressed vapor out of first

compressor stage into the condensing wave rotor and the number of wave cycles per revolution.

5. PERFORMANCE EVALUATION OF CONDENSING WAVE ROTOR INTEGRATED IN A R718 CYCLE

A computer code based on the thermodynamic model described above is generated for performance evaluation of R718 refrigeration cycles enhanced with 3-port condensing wave rotors. The evaporator temperature T_1 and heat rejecter temperature T_3 are commonly fixed by the application. The objective is to get the highest increase in coefficient of performance (COP_{gain}) compared to the baseline cycle. Independent design parameters are the mass flow ratio ($K = \dot{m}_6 / \dot{m}_2$), which relates the mass flow of the cooling cycle to the mass flow of the core cycle, and the pressure ratio of the wave rotor ($PR_W = p_3 / p_2$).

Additional assumptions considered in the thermodynamic model are as follows:

- For comparison of baseline and enhanced cycles, the evaporator and condenser inlet temperatures are considered the same ($T_1 = T_{1b}$ and $T_3 = T_{3b}$).
- Temperature difference across the heat rejecter is kept constant ($T_6 - T_5 = 3$ K).
- Pressure drop in heat exchanger, evaporator, and pipes is neglected.
- The condenser and evaporator outlet states are fully saturated.
- The same polytropic compressor efficiency is used for baseline and enhanced cycles. Its value of 0.72 is obtained by assuming an isentropic efficiency of 0.7 for a compressor with a pressure ratio of 2.
- The superheated vapor is considered as an ideal gas ($\gamma = 1.33$).

- One-dimensional gas-dynamic shock wave equations are used to calculate the flow properties across the moving normal shock wave. Reflected shock waves are not considered.
- The hydraulic efficiency of the pump is 0.9.
- Liquid water is considered as incompressible.

5.1. THE BASELINE PERFORMANCE CALCULATION

In the ideal vapor-compression refrigeration cycle shown in Figure 4, refrigerant from the evaporator flows into the compressor as a saturated vapor, and then it discharges into the condenser as a superheated vapor. The saturated liquid refrigerant at the condenser outlet returns to the evaporator through the expansion valve and then cycle repeats.

Input data for the baseline cycle	
Saturation temperature of the evaporator	T_e
Saturation temperature of the condenser	T_c

Table 5: Input data for the baseline cycle analysis.

As shown in Table 5, saturation temperatures at the evaporator and the condenser are the input data for this analysis. To obtain the COP of the cycle, the thermodynamic states at each location are determined sequentially as follows:

Compressor Inlet (State 1).

$$\begin{aligned} T_1 &= T_e \\ p_1 &= p_{sat}(T_e) \\ h_1 &= h_{sat}(T_e) \end{aligned} \tag{38}$$

Condenser Outlet (State 3_b).

$$T_{3b} = T_c$$
$$p_{3b} = p_{sat}(T_c) \tag{39}$$
$$h_{3b} = h_{sat}(T_c)$$

Compressor Outlet (State 2_b). The cycle overall pressure ratio is calculated by

$$\Pi_b = \frac{p_{3b}}{p_1} \tag{40}$$

and the enthalpy change across the compressor, assuming an average specific heat, is obtained by

$$\Delta h = \left(\frac{1}{\eta_c}\right) C_p T_1 \left[(\Pi_b)^{(\gamma-1)/\gamma}\right] \tag{41}$$

where compressor isentropic efficiency η_C is calculated by assuming a polytropic efficiency of 0.7. Therefore, thermodynamic properties of the compressor outlet are

$$h_{2b} = h_1 + \Delta h$$
$$p_{2b} = p_{3b} \tag{42}$$
$$T_{2b} = T(p_{2b}, h_{2b})$$

Expansion Valve Outlet (state 4_b).

$$h_{4b} = h_{3b}$$
$$p_{4b} = p_1 \tag{43}$$

$$T_{4b} = T(p_{4b}, h_{4b})$$

By definition COP is the ratio between the processed heat at the evaporator ($q_L = h_1 - h_{4b}$) to the work consumed by the compressor ($w_c = h_{2b} - h_{1b}$)

$$COP = \frac{q_L}{w_c} \tag{44}$$

5.2. THE WAVE ROTOR ENHANCED CYCLE PERFORMANCE CALCULATION

As shown in Figure 23 in the enhanced cycle, the superheated vapor leaving the compressor discharges into the wave rotor. The pressure ratio of the compressor is less than that of the baseline engine. After the compression of the superheated vapor in the wave rotor, one portion of the almost saturated water at the wave rotor exit (3) goes to the heat exchanger, while the other portion returns to the evaporator through the expansion valve.

Input data for enhanced cycle	
Saturation temperature of the evaporator	T_e
Saturation temperature of the condenser	T_c
Temperature drop in the condenser	ΔT_c
Mass flow ratio between chilled water cycle and the cooling water cycle	k
Pressure ratio of the baseline cycle	Π_b
Pressure ratio of the wave rotor	PR_w
Hydraulic efficiency of the pump	η_p

Table 6: Input data for the enhanced cycle analysis

The input data for analysis of the enhanced cycle are given in Table 6. To obtain the COP of the enhanced cycle, the thermodynamic states at each location can be obtained sequentially as follows:

Compressor Inlet (State 1). The compressor inlet condition at state 1 is the same as the baseline cycle.

Wave Rotor Outlet (State 3). The wave rotor outlet flow is in the saturation region, very close to the saturated liquid line. Therefore,

$$T_3 = T_c$$
$$p_3 = p_{sat}(T_c) \tag{45}$$

Considering a control volume around the wave rotor, the conservation of mass law gives

$$\dot{m}_2 + \dot{m}_6 = \dot{m}_3 \tag{46}$$

and conservation of energy implies

$$h_2\dot{m}_2 + h_6\dot{m}_6 = h_3\dot{m}_3 \tag{47}$$

Using the definition of mass flow ratio ($K = \dot{m}_6/\dot{m}_2$), Eqs. (46) and (47) can be combined as

$$h_3 = \left(\frac{1}{1+K}\right)(h_2 + h_6 K) \tag{48}$$

The enthalpy at state 6 will be calculated later.

Evaporator Inlet (State 4).

$$p_4 = p1$$

$$h_4 = h_3 \tag{49}$$

$$T_4 = T(p_4, h_4)$$

and the quality of liquid is calculated by

$$x_4 = \frac{h_4 - h_{sat}(T_e)}{h_{sat}(T_e) - h_{sat}(T_c)} \tag{50}$$

Compressor Outlet (State 2). The compressor exit pressure is calculated by

$$p_2 = \frac{\Pi_b}{PR_w} \tag{51}$$

and Equation (41) is used to calculate the enthalpy at the compressor exit, substituting the new value of compressor exit pressure. Therefore,

$$h_2 = h_1 + \Delta h$$

$$T_2 = T(p_2, h_2) \tag{52}$$

Shock Wave Compression (State 2'). As described above, because of the sudden pressure drop from p_6 to p_2, flash evaporation generates a shock wave triggered from the leading edge of the inlet port traveling through the superheated low-pressure vapor, which exists inside the channel. Therefore, the temperature is increased from T_2 to $T_{2'}$ and the pressure is increased from p_2 to $p_{2'} = p_3$. Using moving normal shock relations, temperature increase is calculated by [66]

$$T_{2'} = T_2 \frac{p_3}{p_2} \left[\frac{\frac{p_3}{p2} + \frac{\gamma+1}{\gamma-1}}{1 + \frac{\gamma+1}{\gamma-1}\frac{p_3}{p2}} \right] \tag{53}$$

and

$$p_{2'} = p_3$$
$$h_{2'} = h(T_{2'}, p_{2'}) \tag{54}$$

Pump Outlet (State 5). As stated above, the pressure (p_5) provided by the pump in the cooling water cycle is used to generate the pressure ratio p_6 / p_2 required to trigger the desired shock wave. Therefore,

$$\Delta p = (h_{2'} - h_2)\frac{\rho_5}{K} \tag{55}$$

where liquid water is considered incompressible; therefore, $\rho_5 = \rho_3 = \rho(T_3, p_3)$. Thus,

$$p_5 = p_3 + \Delta p \tag{56}$$

and the enthalpy increase by the pump is

$$\Delta h = \frac{\Delta p}{\rho_5 \eta_h} \tag{57}$$

where η_h is hydraulic efficiency of the pump. Therefore,

$$h_5 = h_3 + \Delta h \tag{58}$$

$$T_5 = T(p_5, h_5)$$

Heat Exchanger (Cooling-Tower) Outlet (State 6). For the indirect cooling-tower, the temperature drop across the cooling-tower is assumed ΔT_c (see Table 6); therefore,

$$T_6 = T_5 - \Delta T_c$$

$$p_6 = p_5 \tag{59}$$

$$h_6 = h(T_6, p_6)$$

Finally, COP for the enhanced cycle is obtained by

$$COP = \frac{q_L}{w_c + w_p K} \tag{60}$$

where

$$\begin{aligned} q_L &= h_1 - h_4 \\ w_L &= h_2 - h_1 \\ w_p &= h_5 - h_3 \end{aligned} \tag{61}$$

5.3. PERFORMANCE RESULTS AND DISCUSSIONS

Figure 33 shows the percentage increase in COP relative to baseline versus the evaporator temperature (T_1) for different mass flow ratios K. By increasing evaporator temperature T_1, the COP of the wave-rotor-enhanced cycle is increased relative to the COP of the baseline cycle. This trend is seen until the compressor pressure ratio in the enhanced cycle ($\Pi_c=p_2/p_1$) is reduced to a value that is equal to the wave rotor pressure ratio ($\Pi_c = PR_W$). After that, the relative COP_{gain} drops dramatically.

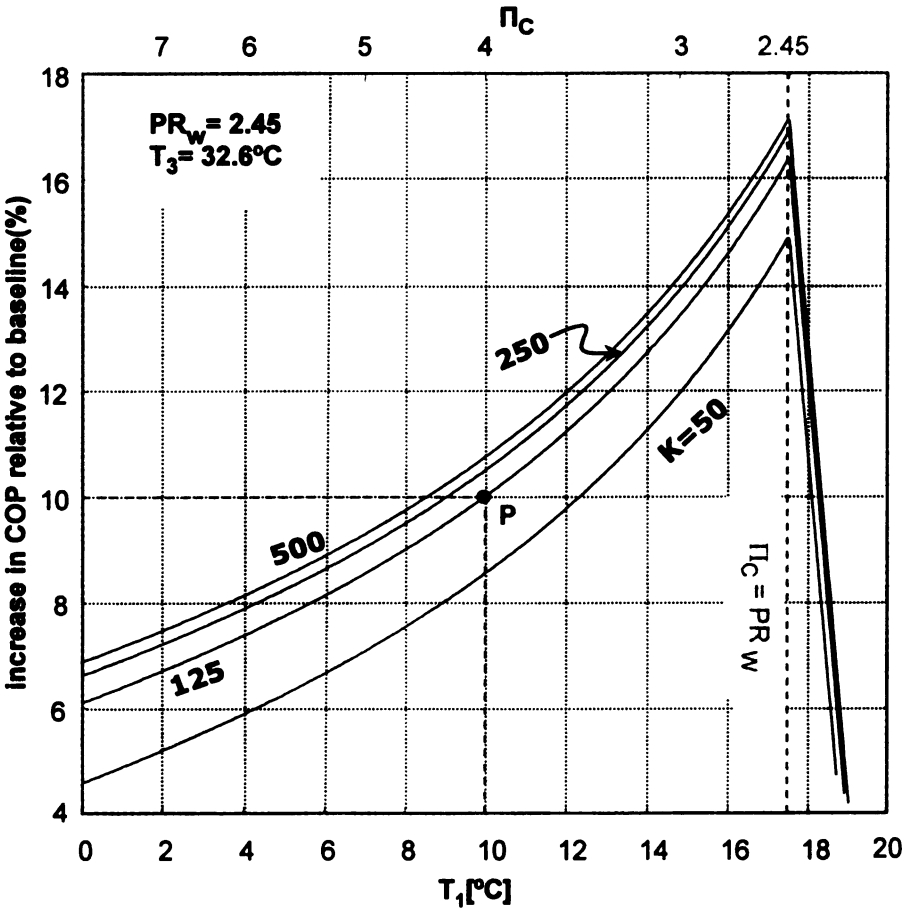

Figure 33: Relative COP increase versus evaporation temperature for different mass flow ratios

Figure 34 represents the percentage increase in COP relative to baseline versus mass flow ratio *K* for different evaporator temperatures, such as a side view of Figure 33.

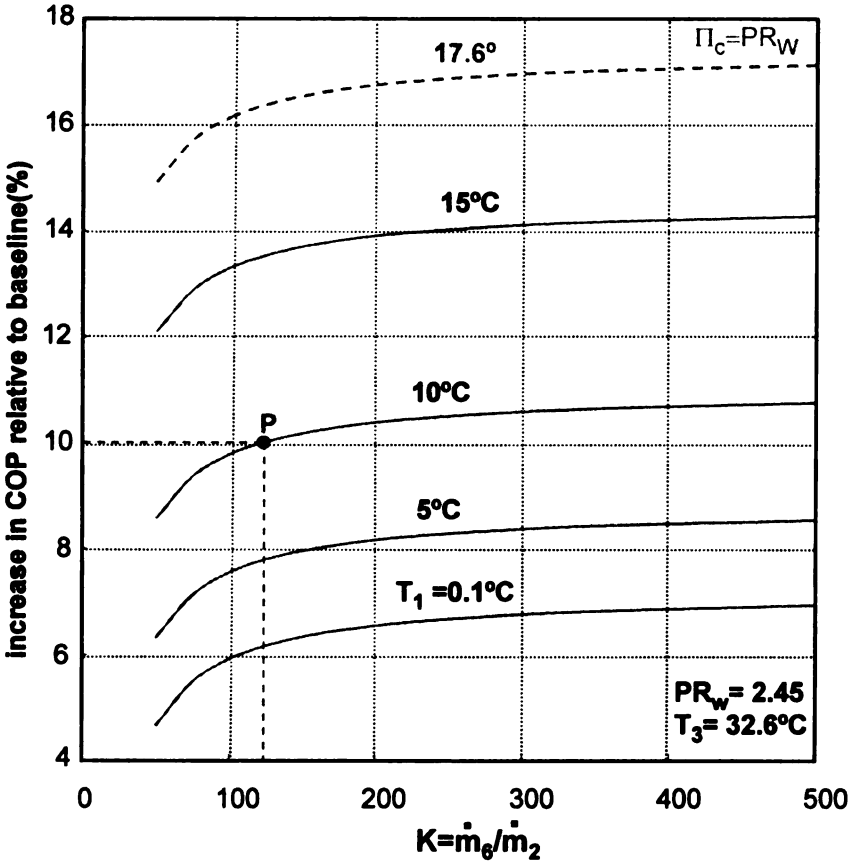

Figure 34: Relative COP increase versus mass flow ratio for different evaporation temperatures

It shows only the increasing branches of Figure 33 up to an evaporation temperature where the pressure ratio of the turbocompressor is reduced to the value of the wave rotor pressure ratio. Increasing the mass flow ratio above 200 appears as ineffective according to Figure 34.

Figure 35 shows the effect of the wave rotor pressure ratio (PR_W) on the percentage increase in COP relative to baseline for different mass flow ratios *K*. Each curve has a maximum point that indicates the best choice of wave rotor

pressure ratio for the given system specifications. The location of this point depends on several parameters including the hydraulic efficiency of the pump, compressor polytropic efficiency, evaporator temperature, and temperature lift $T_3 - T_1$, but not the mass flow ratio.

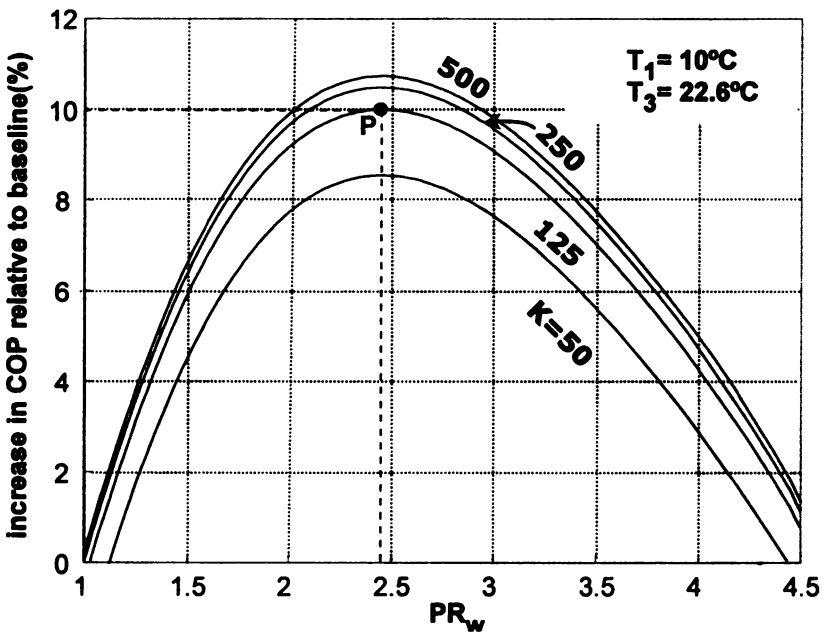

Figure 35:Relative COP increase versus the wave rotor pressure ratio for different mass flow ratios.

One common characteristic shown in Figure 33 to Figure 35 is that a continued increase of the independent value does not always increase the COP_{gain}. Although Figure 35 shows this effect for the wave rotor pressure ratio, Figure 33 reveals a growing gradient of COP_{gain} up to the point where further increase of evaporator temperature actually reduces COP_{gain}. A similar trend can be seen in Figure 34 where the curves have an asymptotic behavior for increased mass flow ratio.

Figure 36 shows the heat rejecter temperature T_3 versus evaporator temperature for different wave rotor pressure ratios and a constant relative

COP_{gain} of 10%. The figure indicates that there are several options for the wave rotor pressure ratio to obtain a certain relative COP_{gain}. However, only the optimum pressure ratio of 2.45 yields the highest temperature lift.

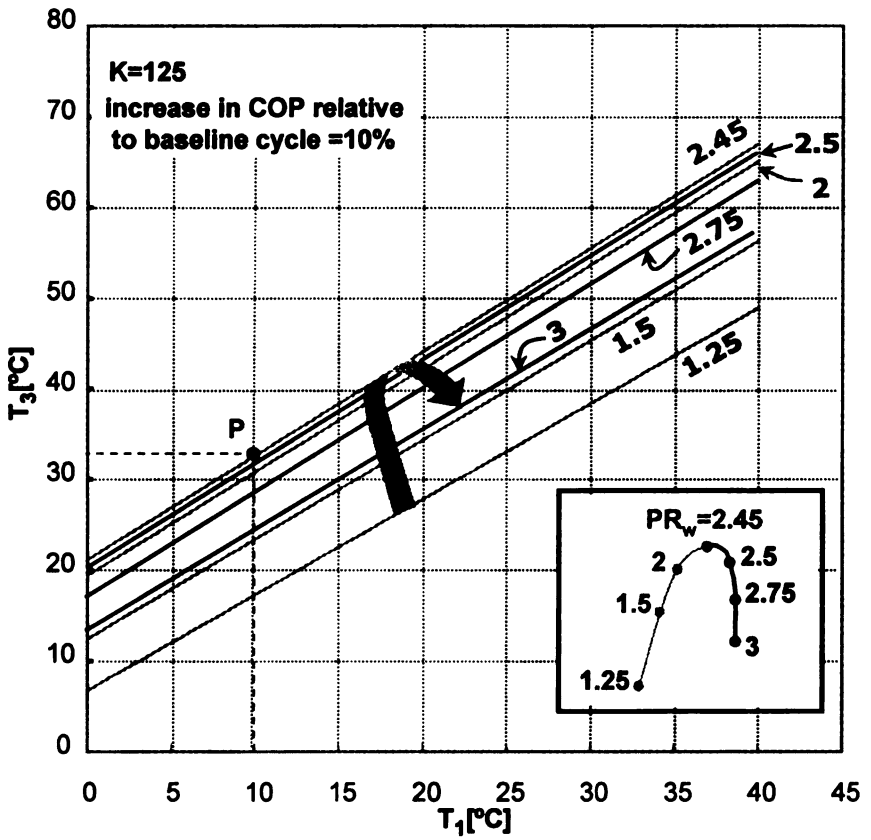

Figure 36: Heat rejecter temperature versus evaporator temperature for different wave rotor pressure ratios.

Figure 37 is a performance map of the enhanced cycle. Each point on this plot shows the maximum COP_{gain} that can be obtained by the optimum choice of PR_W for a given evaporator temperature and temperature lift. The constant PR_W lines indicate the optimum PR_W that yields the highest possible COP_{gain} indicated by constant maximum COP_{gain} lines.

State	P [pa]	T [°C]	h [kJ/kg]	s [kJ/kg.K]
1_b	1227	10.0	2519.90	8.90
2_b	4917	179.9	2840.90	9.14
3_b	4917	32.6	136.50	0.47
4_b	1227	10.0	136.50	0.49

Table 7: Calculated baseline cycle state values for the selected optimum point P

State	P [pa]	T [°C]	h [kJ/kg]	s [kJ/kg.K]
1	1227	10.0	2519.90	8.90
2	2007	61.9	2616.61	8.98
2'	4917	154.0	2791.27	9.03
3	4917	32.6	143.77	0.49
5	6307	34.7	145.33	0.50
6	6307	31.7	123.99	0.43
8	1227	10.0	143.77	0.51

Table 8: Calculated enhanced-cycle state values for the selected optimum point P

In this performance plot of optimized points, an arbitrary optimum point P is marked. This point is used to show the connection between all the performance graphs. However, it is the only optimum point in the performance plots of Figure 33 to Figure 36. All other points of these plots are not found in

Figure 37 because they show a smaller COP_{gain} than the points in

Figure 37. The calculated state values for the optimum point *P* are tabulated in Table 7 and Table 8.

be seen in the performance map of the optimized points (Figure 37) by moving point *P* to the right along constant PR_W line of 2.45. However, for temperature lifts below ~15 K (above maximum COP_{gain} of ~16%) this effect is reversed such that the maximum COP_{gain} decreases with increasing evaporator temperature.

Figure 35 showed that for a given mass flow ratio and a combination of evaporation and heat rejecter temperatures maximum COP_{gain} exists. Since point *P* is at the maximum of the dome, it also appears in Figure 37.

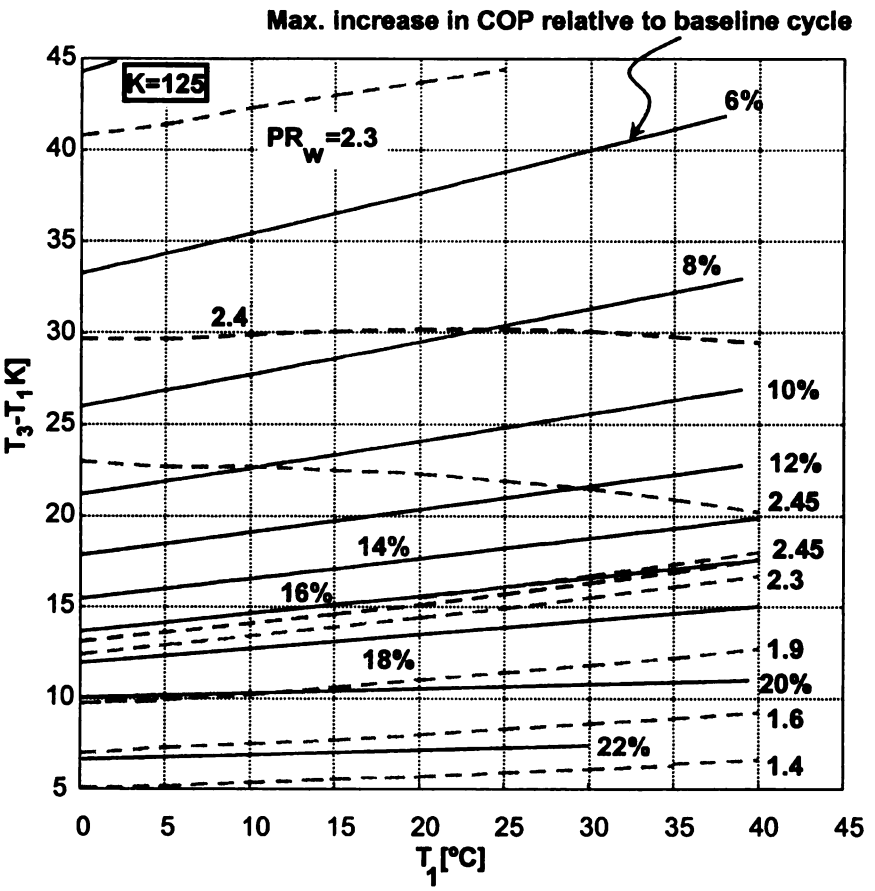

Figure 37: Performance map: maximum performance increase and optimum wave rotor pressure ratios.

The following results can be obtained from the performance map of optimized points:

1. The lower the temperature lift, the higher the relative maximum COP_{gain} of the enhanced cycle is.

2. The maximum optimum PR_W for a condensing 3-port wave rotor is about 2.51.

3. Although below a temperature lift of approximately 18 K, the optimum PR_W increases with the temperature lift and decreases slightly for higher temperature lifts. This trend shows a rapidly decreasing gradient with increasing temperature lift.

4. The slope of constant COP_{gain} lines increases as the temperature lift increases, showing that an increase of evaporation temperature is even more beneficial for the enhanced cycle, especially for greater temperature lifts as it is already the case for the R718 baseline cycle.

5. EXPERIMENTAL STUDY OF SHOCK WAVE VISUALIZATION USING SCHLIEREN METHOD

5.1. SCHLIEREN VISUALIZATION TECHNIQUE

Schlieren methods visualize changes in the refractive index of transparent fluids, and have applications in many areas of flow visualization especially shock wave studies. The Schlieren method holds a special place in flow visualization because it produces a natural, easily interpretable image of the refractive index of gradient fields. A Schlieren instrument records changes in the refractive index distribution of transparent media-like air flows. The refractive index distribution can then be related to density, temperature, or pressure distributions within the flow. The basic system uses light with parallel rays with a plane wave front. In order to have parallel rays, the source is passed through a thin slit, and then collimated by either a mirror or a lens. The collimated light is passed through the flow and then brought to focus. If the flow is steady, the focal spot is an image of the source slit; but if any turbulence exists, scintillation will occur. In order to intensify the effect, a knife edge is placed in front of the camera, positioned to block off about half of the light. In uniform flow this will simply make the photograph half as bright. However in turbulent flow the light's path will be bent, because of changes in the index of refraction caused by density gradients. In this case some of the light that would otherwise be seen in the camera will instead hit the knife-edge, and some that would normally be blocked will become visible. The result is a set of lighter and darker patches corresponding to different densities in the fluid. A simple Schlieren system can be built with a single mirror

with a long focal length; telescope mirrors can be used for this purpose. The camera and light source are placed close together on either side of the focus, and are aimed at the mirror (Figure 38).

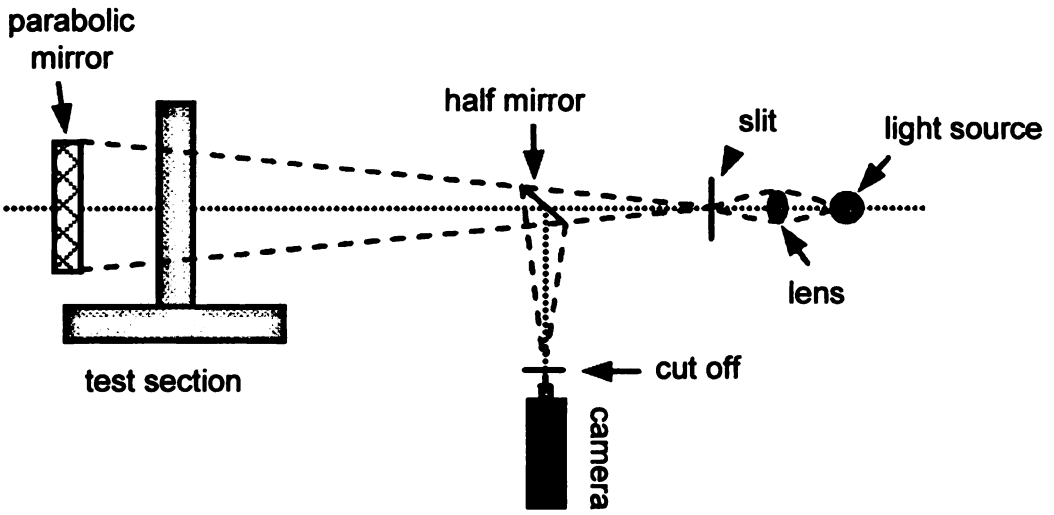

Figure 38: Diagram of Schlieren setup for shock visualization

5.2. SCHLIEREN TECHNIQUE FOR VISUALIZATION OF SHOCK WAVE IN A SMALL SIZE WAVE ROTOR

In order to understand the shock wave propagation in wave rotor channels and examine the effectiveness of Shlieren technique for shock visualization in wave rotor channels, experimental equipment was built at University of Tokyo to study the fluid flow inside a single channel of a miniaturized wave rotor. For visualization, the Schlieren technique was used to study the shock wave traveling in a miniaturized channel of a wave rotor. Figure 39 shows the Schlieren setup at University of Tokyo.

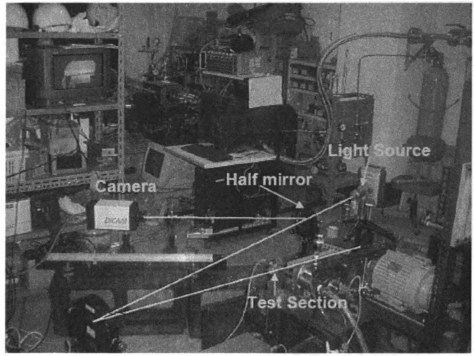

Figure 39: Schlieren setup at University of Tokyo for shock wave visualization in a single channel of a wave rotor

In this special design, the design of a stationary single channel is so that it simulates the flow dynamics of a rotating channel. For this purpose, the buffer chamber is fixed, and high pressure air coming from a screw compressor is supplied constantly. To introduce the high pressure air to the test section periodically, a rotor with inlet and outlet ports is rotating. A pressure transducer is used to monitor the pressure change at the end of the tube (Figure 40). Also, in order to trigger the camera, the passage openings were determined using a laser which was pointing at the rotating shaft. The rotating shaft was painted so that it was half black and white. Therefore, the reflection of the laser from these two colored areas was different and could be detected.

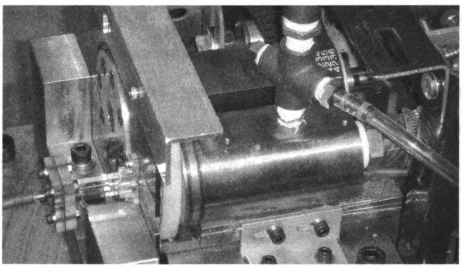

Figure 40: Especial design for fluid study in a single channel of a wave rotor (University of Tokyo)

To study the flow inside the miniaturized wave rotors, two glass-made cells with the lengths of 38 mm and 165 mm with rectangular cross sectional area of 3mm by 3mm were used. Figure 41 shows a photograph of the 38 mm glass-cell used for this study.

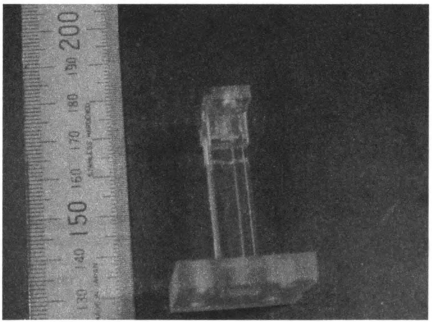

Figure 41: A 38 mm Glass-made channel for Shock Visualization

In the wave rotors τ is defined as the ratio of passage opening time and the wave travel time. To compare the pressure distribution at the end wall of the test sections, cases with the same τ value were considered. Rotor rotational speed of 40 Hz for the short cross section is corresponding to the 10 Hz rotor rotational speed for the long test section. As shown in Figure 42, the gradient of pressure jump for both test sections up to pressure ratio of 0.25 MPa is the same. This pressure ratio is corresponding to the primary shock wave. After this point the short cross section has sharper gradient. This difference in the gradient could be because of the size scale which results in different shock interactions such as arrival of expansion wave. The fluctuations in the short cross section are mainly because of the oscillatory nature of pressure injection by the compressor.

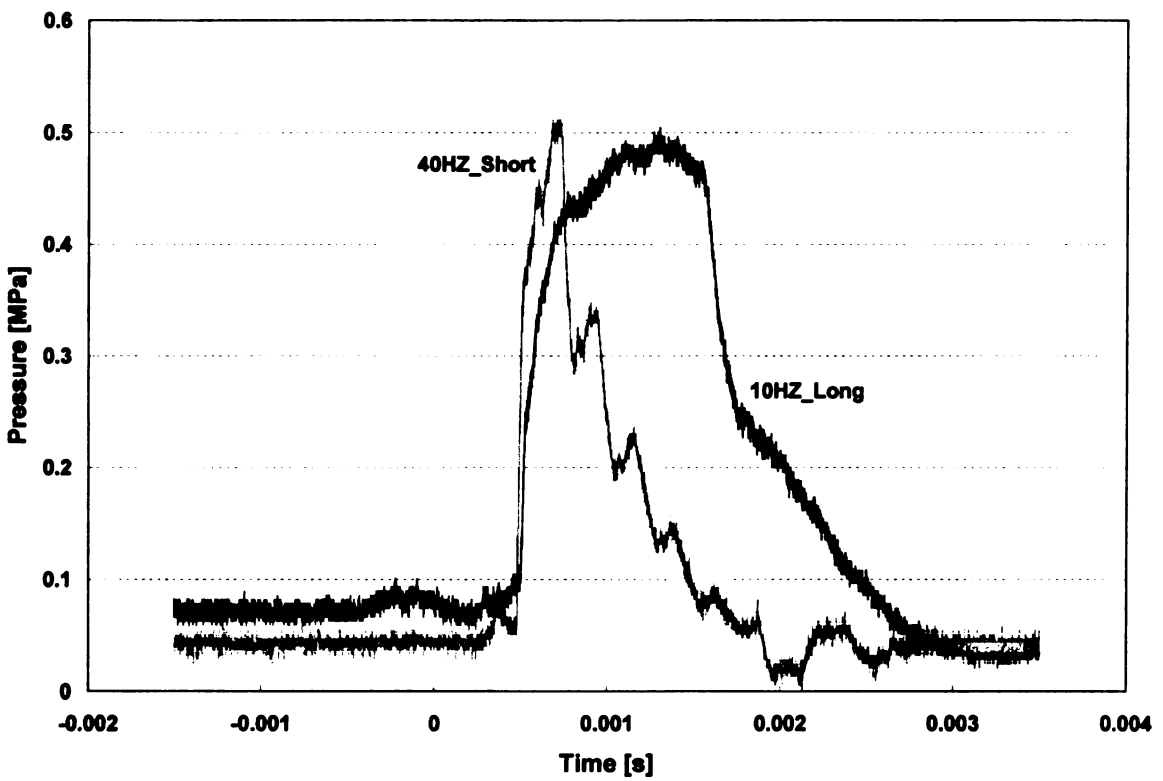

Figure 42: Pressure distribution at the end wall of the short and long test sections (π =2.5, A= 3*3)

Figure 43 shows the picture obtained using the Schlieren method for the 38mm test section. In this picture, the primary and secondary shock waves are clearly observed. The speed of the primary shock is 470 m/s and the secondary shock 315 m/s which are slightly higher than the calculated values. This could be because of the error of measurement devices such as the pressure gage. In Figure 42, the start of pressure jump is at 470 microseconds. This fact can be observed in Figure 43 as the primary shock wave reaches to the end and is reflected at 470 microseconds.

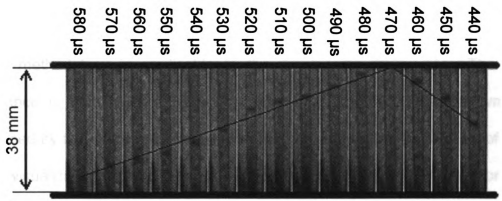

Figure 43: Shock wave visualization using Schlieren method for a 38 mm test section (π =2.5, N=40 Hz, A= 3*3)

Figure 44 is the same observation for the longer test section. During the experiment, it was observed that the higher the rotational speed, the easier it was to visualize the shock wave.

Also, for the longer test section, visualization of the primary shock using Schlieren method was not possible, and as it can be seen in the picture only the secondary shock is observable.

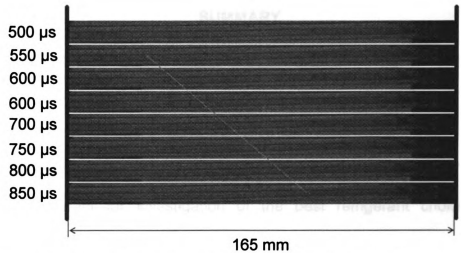

Figure 44: Shock wave visualization using Schlieren Method for 165 mm Test Section ((π =2.5, N=40 Hz, A= 3*3)

Although the Schlieren technique was only used in the gaseous phase, the same methodology is applicable in the condensing wave rotor. The major difference is that in the condensing wave rotor the high pressure vapor is produced by the means of flash evaporation. The experimental analysis of shock wave visualization in the channels of a condensing wave rotor remains for future work.

SUMMARY

In the present study, the advantages of cycles working with water as a refrigerant (R718) and challenges involved with designing them are mentioned. A code has been developed to compare R718 with other refrigerants in *p-h*, *T-s*, and *p-T* diagrams. Also, the code generates the COP isolines for R718 and a selected refrigerant for investigation of the best refrigerant choice in any operating point.

To enhance the turbocompression and improve the efficiency of R718 cycles, the novel concept of 3-port condensing wave rotors integrated in R718 compression refrigeration cycles is investigated. The condensing wave rotor employs pressurized water to pressurize, desuperheat, and condense the superheated vapor coming from the compressor, all in one dynamic process. The schematic *p-h* and *T-s* diagrams of the external processes and the wave and phase-change diagram of the internal process are discussed. Flash evaporation, shock wave compression, desuperheating, and condensation phenomena inside the wave rotor channels are described. A computer code based on a thermodynamic model is developed to evaluate the performance improvement of R718 enhanced cycles. The effect of some key parameters on the performance enhancement is demonstrated as an aid for optimization. Finally, a performance map showing the optimized points of the enhanced cycle is presented. The presented results show an additional improvement of the COP of up to 22% by using the 3-port condensing wave rotor. Besides the performance enhancement, the condensing wave rotor allows lower compressor pressure ratios for the same

temperature lift or increases the temperature lift without changing the compressor.

This wave rotor is a simple drum, easy to manufacture, rotating at relatively low speed. Because it performs compression, desuperheating, and condensation in one compact device, it can reduce the size and cost of modern state-of-the-art R718-chillers that now employ high-tech multistage compressors, intercooler, and relatively bulky condensers.

In the last chapter, as a proof of concept, an experimental investigation by the author for flow visualization in the channels of a wave rotor is described. The shock wave propagation inside the channels of a small size wave rotor is visualized using Shlieren technique. The same concept is suggested for future work to visualize the shock propagation inside channels of a condensing wave rotor.

REFERENCES

[1] Yunas, C., Boles, M, 1998," Thermodynamics: An Engineering Approach" Highstown: McGraw Hill.

[2] Rowland, F. S., Molina, M. J., 1994 "Ozone Depletion: 20 Years after the Alarm," Chemical and Engineering News, Vol. 72, pp: 8-13.

[3] U.S. Environmental Protection Agency Web Site: Health Effects of Overexposure to the Sun http://www.epa.gov/sunwise/uvandhealt.html.

[4] Ozone Secretariat United Nations Environment Programme, 2001, The Vienna Convention for the Protection of the Ozone Layer, UNON, Kenya.

[5] Anderson, S. O., Sarma, K. M., 2002, Protecting the Ozone Layer, Earthscan Publications Ltd, US.

[6] Griffith, G., 1993, "Alternate Refrigerants for the Refrigeration Industry" ASHREA-NIST Refrigerants Conference, pp.19-28.

[7] Parson, E. A., 2003, Protecting the Ozone Layer: Science and Strategy, Oxford University Press, New York.

[8] Gerwen R. J. M., Verchoor M. J. E., 1997 "Air as Refrigerant: Prospects and Challenges," IEA Workshop Proceedings, Annex 22, Gatlinburg, Tennessee, pp: 87-93.

[9] Giles, G. R., Hunt, R. G., and Stevenson, G. F., 1997 "Air as a Refrigerant for the 21st Century," Proceedings of ASHRAE-NIST Conference, Gaithersburg, US, pp: 96-103.

[10] Vrinat, G., 2003 "Ammonia: Technical Characteristics, Regulations and Impact on the Environment," Chaud Froid Plomb.(French Journal), 658, pp: 55-60.

[11] The U.S. Occupational Health and Safety Administration (OSHA) Laws: 1998 - 06/26/1998 - Storage and Handling of Anhydrous Ammonia (29 CFR 1910.111), www.osha.gov.

[12] Granryd, E., 2001 "Hydrocarbons as Refrigerants: an Overview," International Journal of Refrigeration, 24, No. 1, pp: 15-24.

[13] Pearson, S. F., 1996 "Uses of Hydrocarbon Refrigerants," International Institute of Refrigeration, Proceeding of Aarhus Meeting, pp: 439-446.

[14] Orbitz, T. M., Li, D., Groll E. A., 2003 "Evaluation of the Performance of Potential of CO2 as a Refrigerant in Air-to-Air Air Conditioners and Heat Pumps: System Modeling and Analysis," ARTI-21CR/610-10030.

[15] Hans, J. H., Hwang, Y., and Radermacher R., 2002 "Options for A Two-Stage Transcritical Carbon Dioxide Cycle," Proceeding of IIR conference Commissions B1, B2, E1 and E2, Guangzhou, China, pp: 158-164.

[16] Müller N., 2002, "Turbo Chillers using Water as a Refrigerant" ASME Process Industry Division PID Newsletter, Fall 2002, p 3.

[17] Kharazi, A. A., Akbari, P., and Müller, N., 2004, "An Application of Wave Rotor Technology for Performance Enhancement of R718 Refrigeration Cycles" 2nd International Energy Conversion Engineering Conference, AIAA Paper 2004-5636.

[18] Kharazi, A. A., Akbari, P., and Müller, N., 2004, "Performance Benefits of R718 Turbo-Compression Cycles Using a 3-Port Condensing Wave Rotors" 2004 International Mechanical Engineering Conference, ASME Paper IMECE2004- 609926.

[19] Yuan, Q.S., Blaise, J.C., 1998, "Water - A Working Fluid for CFC Replacement," Rev. Int. Froid, 11, pp. 243-248.

[20] Kilicarslan, A., Müller, N., 2004, "COPs of R718 in Comparison with Other Modern Refrigerants" The First Cappadocia International Mechanical Engineering Symposium, Cappadocia, Turkey.

[21] Rossi, F., Mastrullo, R., 1991, "Working Fluids Thermodynamic Behavior for Vapor Compression Cycles" Applied Energy 0306-2619, pp.163-180.

[22] Albring, P., 1994, "Water as A Refrigerant in Refrigeration Plants with Mechanical Compression" ISSN 0151-1637, New Applications of the Natural Working Fluids in Refrigeration and Air Conditioning, IIR, Hannover, pp. 735-742.

[23] Albring, P., Heinrich, G., 1998, "Turbo Chiller with Water as Refrigerant" Natural Working Fluids '98, IIR, Oslo, pp. 93-103.

[24] Lachner, B., Nellis, G., and Reindl, D., 2004, "An Investigation into the Feasibility of the Use of Water as a Refrigerant" International Refrigeration and Air Conditioning Conference, Purdue, R160, pp. 1-8.

[25] Müller, N., 2001, "Design of Compressor Impellers for Water as a Refrigerant" ASHRAE Transactions, 107, pp. 214-222.

[26] Wobst, E., Kalitzin, N., and Apley, R., 2005, "Turbo Water Chiller with Water as Refrigerant" Seventeenth International Compressor Engineering Conference at Purdue, C129.

[27] ILK Dresden, Germany, Company Brochure, 2004, "R718-Turbo-Chiller System Dimensions" R718-Turbo-A626 (ATV110/1-25-52 and ATV110/3-21-52).

[28] Gupta, R. P., Linton, J. W., and Snelson, W. K., 1994 "R&D Test facility to Develop Systems Using Water as Refrigerant,", IEA, Annex 22 / IEA HPP, Trondheim Workshop Proc., pp: 203-215.

[29] Wobst, E., Kalitzin, N., Apley, R., 2004 "Turbo Water Chiller with Water as Refrigerant", International Compressor Engineering Conference at Purdue, Paper C129.

[30] Paul, J., Jahn E., 1996, "Water Chilling and Ice Making with Water as Refrigerant," Preceedings of the International Conference on Ozon Protection Technologies, Washington, USA, pp: 955-960.

[31] Nyvad J., Elefsen F., 1993, "Energy Efficient Cooling by Use of Cycloid Water Vapour Compressor," IIR, Proceedings of Ghent Meeting, pp: 67-74.

[32] Hackensellner T., Jurisch C., 1994, "Water: A Working Fluid for a Compression Heat Pump with a Liquid Ring Compressor," IIR, Proceedings of Hanover Meeting, pp: 755-764.

[33] Grazzini, G., D'Albero, M. 1998, "A Jet-Pump Inverse Cycle with Water Pumping Column," Proceeding of Meeting of Commissions B1, B2, E1, E2, IIR, Oslo, pp. 63-68.

[34] Wight, S. E., Yoshinaka, T., Le Drew, B. A., and D'Orsi, N. C., 2000 "The Efficiency Limits of Water Vapor Compressors," ARTI-21CR/605-10010-01.

[35] Paul, J., 1998 "District Cooling with Water as Refrigerant Combined with Energy Storage Systems," IIF-IIR, Commission B2,with B1,E1&E2, Oslo, Norway, pp.82-92.

[36] Zimerman, Z., 1994 "Development of Large Capacity High Efficiency Mechanical Compression (MVC) Units," Desalination, 96, pp: 51-58.

[37] Madsboll, M. S., Minds, G., Nyvad, J., and Elefsen, F., 1994 "The State of Art for Water Vapour Compressors and Cooling Plants Using Water as Refrigerant," Proc. Hanover Meet., IIR, pp: 743-758.

[38] Albring, P., Burandt B.,and Schenk, N., 2002, "Water Vapour Compression: Application and Outlook," KI Luft Kältetech DE, 38, n.6, pp: 276-281.

[39] Kühnl-Kinel, J., 1997 "New Age Water Chillers with Water as Refrigerant," CERN, Geneva.

[40] Weber, H. E., 1995, Shock Wave Engine Design, John Wiley and Sons, New York.

[41] Weber, H. E., 1986, "Shock-Expansion Wave Engines: New Directions for Power Production" ASME Paper 86-GT-62.

[42] Akbari, P., Kharazi, A. A., and Müller, N., 2003, "Utilizing Wave Rotor Technology to Enhance the Turbo Compression in Power and Refrigeration Cycles" 2003 International Mechanical Engineering Conference, ASME Paper IMECE2003-44222.

[43] Akbari, P.,Nalim, M. R., and Müller, N., 2004, "A Review of Wave Rotor Technology and Recent Developments" *2004 International Mechanical Engineering Conference*, ASME Paper IMECE2004-60082, USA.

[44] Taussig, R. T., Hertzberg, A., 1984, "Wave Rotors for Turbomachinery" Winter Annual Meeting of the ASME, edited by Sladky, J. F., Machinery for Direct Fluid-Fluid Energy Exchange, AD-07, pp. 1-7.

[45] Shreeve, R. P., Mathur, A., 1985, Proceeding ONR/NAVAIR Wave Rotor Research and Technology Workshop, Report NPS-67-85-008, Naval Postgraduate School, Monterey, CA.

[46] Paxson, D. E., 1995, "Comparison Between Numerically Modeled and Experimentally Measured Wave-Rotor Loss Mechanism" Journal of Propulsion and Power, 11, No. 5, pp. 908-914.

[47] Paxson, D. E., 1996, "Numerical Simulation of Dynamic Wave Rotor Performance" Journal of Propulsion and Power, 12, No. 5, pp. 949-957. See also AIAA Paper 95-2800 and NASA TM 106997.

[48] Wilson, J., Paxson, D. E., 1996, "Wave Rotor Optimization for Gas Turbine Topping Cycles" Journal of Propulsion and Power, 12, No. 4, pp. 778-785.

[49] Welch, G. E., Jones, S. M., and Paxson, D. E., 1997, "Wave Rotor-Enhanced Gas Turbine Engines" Journal of Engineering for Gas Turbines and Power, 119, No. 2, pp. 469-477.

[50] Welch, G. E., 1997, "Macroscopic Balance Model for Wave Rotors" Journal of Propulsion and Power, 13, No. 4, pp. 508-516.

[51] Welch, G. E., 1997, "Two-Dimensional Computational Model for Wave Rotor Flow Dynamics" Journal Engineering for Gas Turbines and Power, 119, No. 4, pp. 978-985. See also ASMA Paper 96-GT-550 and NASA TM 107192.

[52] Wilson, J., 1998, "An Experimental Determination of Loses in a Three-Port Wave Rotor" Journal of Engineering for Gas Turbines and Power, 120, pp. 833-842.

[53] Paxson, D. E., Nalim, M. R., 1999, "Modified Through-Flow Wave-Rotor Cycle with Combustor Bypass Ducts" Journal of Propulsion and Power, 15, No. 3, pp. 462-467.

[54] Welch, G. E., 2000, "Overview of Wave-Rotor Technology for Gas Turbine Engine Topping Cycles" Novel Aero Propulsion Systems International Symposium, The Institution of Mechanical Engineers, pp. 2-17.

[55] Smith, C. F., Snyder, P. H., Emmerson, C. W., Nalim M. R., 2002, "Impact of the Constant Volume Combustor on a Supersonic Turbofan Engine" AIAA Paper 2002-3916.

[56] Akbari, P., and Müller, N., 2005, "Wave Rotor Research Program at Michigan State University" 41st AIAA/ASME/SAE/ASEE Joint Propulsion Conference and Exhibit, AIAA Paper 2005-3844.

[57] Saury, D., Harmand, S., and Siroux, M, 2001, "Experimental Study of Flash Evaporation of Water Film" International Journal of Heat and Mass Transfer, No. 45, pp. 3447-3457.

[58] Kentfield, J. A. C., 1998, "Wave Rotors and Highlights of Their Development," AIAA Paper 98-3248.

[59] Burghard, H., 1929, German Patent 485386.

[60] Darrieus, G., 1950, "Pressure Exchange Apparatus," U.S. Patent 2526618.

[61] Kentfield, J. A. C., 1993, *Nonsteady, One-Dimensional, Internal, Compressible Flows*, Oxford University Press, Oxford.

[62] Gyarmathy, G., 1983, "How Does the Comprex® Pressure-Wave Supercharger Work?" SAE Paper 830234.

[63] Zehnder, G., Mayer, A. and Mathews, L., 1989, "The Free Running Comprex®," SAE Paper 890452

[64] Kharazi, A. A., Akbari, P., and Müller, N., 2004, "Preliminary Study of a Novel R718 Turbo-Compression Cycle Using a 3-Port Condensing Wave Rotor" 2004 International ASME Turbo Exposition, ASME Paper GT2004-53622.

[65] Miyatake, O., Murakami, K., and Kawata, Y., 1973, "Fundamental Experiments with Flash Evaporation" Heat Transfer Jpn., Res. 2, pp. 89-100.

[66] Anderson, J. D., 2003, Modern Compressible Flow, McGraw hill, Third Edition.

[67] Daneshyar, H., 1976, "One-Dimensional Compressible Flow" Pergamon Press.

[68] Grlffith, G., 1993 "Alternate Refrigerants for the Refrigeration Industry," ASHREA-NIST Refrigerants Conference, pp.19-28.

[69] Parson, E. A., 2003, Protecting the Ozone Layer: Science and Strategy, Oxford University Press, New York, US.

[70] Albring, P., Heinrich, G., 1996, "R718 Heat Pumps: Applications for Natural Refrigerants," IIR, Aarhus, pp. 553-558.

[71] Müller, N., 2001 "Design of compressor impellers for water as a refrigerant" ASHRAE Transaction 107, pp: 214-222.